

1 Pre-print

2

3 Solarino S., Malusa M. G., Eva E., Guillot S., Paul A. et al. (2018)

4

5 Mantle wedge exhumation beneath the Dora-Maira  
6 (U) HP dome unravelled by local earthquake  
7 tomography (Western Alps).

8

9 Lithos, 296, 623-636.

10

11 <https://doi.org/10.1016/j.lithos.2017.11.035>

12

13 Mantle wedge exhumation beneath the Dora-Maira (U)HP dome  
14 unravelled by local earthquake tomography (Western Alps)

15 Stefano Solarino<sup>1</sup>, Marco G. Malusà<sup>2</sup>, Elena Eva<sup>1</sup>, Stéphane Guillot<sup>3</sup>, Anne Paul<sup>3</sup>, Stéphane  
16 Schwartz<sup>3</sup>, Liang Zhao<sup>4</sup>, Coralie Aubert<sup>3</sup>, Thierry Dumont<sup>3</sup>, Silvia Pondrelli<sup>5</sup>, Simone Salimbeni<sup>5</sup>,  
17 Qingchen Wang<sup>4</sup>, Xiaobing Xu<sup>4</sup>, Tianyu Zheng<sup>4</sup>, Rixiang Zhu<sup>4</sup>

18 <sup>1</sup> *Istituto Nazionale di Geofisica e Vulcanologia, CNT, Genova, Italy*

19 <sup>2</sup> *Department of Earth and Environmental Sciences, University of Milano-Bicocca, Milano, Italy*

20 <sup>3</sup> *Univ. Grenoble Alpes, Univ. Savoie Mont-Blanc, CNRS, IRD, IFSTTAR, ISTerre, Grenoble, France*

21 <sup>4</sup> *Institute of Geology and Geophysics, Chinese Academy of Sciences, Beijing, China*

22 <sup>5</sup> *Istituto Nazionale di Geofisica e Vulcanologia, Bologna, Italy*

23 Authors for correspondence : S. Solarino and M.G. Malusà (stefano.solarino@ingv.it; marco.malusa@unimib.it)

24 **Abstract**

25 In continental subduction zones, the behaviour of the mantle wedge during exhumation of  
26 (ultra)high-pressure [(U)HP] rocks provides a key to distinguish among competing exhumation  
27 mechanisms. However, in spite of the relevant implications for understanding orogenic evolution, a  
28 high-resolution image of the mantle wedge beneath the Western Alps is still lacking. In order to fill  
29 this gap, we perform a detailed analysis of the velocity structure of the Alpine belt beneath the  
30 Dora-Maira (U)HP dome, based on local earthquake tomography independently validated by  
31 receiver function analysis. Our results point to a composite structure of the mantle wedge above the  
32 subducted European lithosphere. We found that the Dora-Maira (U)HP dome lays directly above  
33 partly serpentinized peridotites ( $V_p \sim 7.5$  km/s;  $V_p/V_s = 1.70-1.72$ ), documented from  $\sim 10$  km  
34 depth down to the top of the eclogitized lower crust of the European plate. These serpentinized  
35 peridotites, possibly formed by fluid release from the subducting European slab to the Alpine  
36 mantle wedge, are juxtaposed against dry mantle peridotites of the Adriatic upper plate along an  
37 active fault rooted in the lithospheric mantle. We propose that serpentinized mantle-wedge  
38 peridotites were exhumed at shallow crustal levels during late Eocene transtensional tectonics, also

39 triggering the rapid exhumation of (U)HP rocks, and were subsequently indented under the Alpine  
40 metamorphic wedge in the early Oligocene. Our findings suggest that mantle-wedge exhumation  
41 may represent a major feature of the deep structure of exhumed continental subduction zones. The  
42 deep orogenic levels here imaged by seismic tomography may be exposed today in older (U)HP  
43 belts, where mantle-wedge serpentinites are commonly associated with coesite-bearing continental  
44 metamorphic rocks.

45 **Keywords:** continental subduction; ultra-high-pressure metamorphism; mantle wedge exhumation;  
46 peridotite serpentinization; local earthquake tomography; Western Alps

47 **Highlights:**

- 48 - High-resolution image of the seismic velocity structure of the Alpine mantle wedge
- 49 - First geophysical evidence of mantle-wedge exhumation during continental subduction
- 50 - Mantle wedge exhumation is favoured by upper plate divergent motion

51 **1. Introduction**

52 Exhumed (ultra)high-pressure [(U)HP] rocks bear compelling evidence of the interaction  
53 between subducting plates and the overlying mantle wedge (Carswell and Compagnoni, 2003;  
54 Hacker et al., 2006; Ferrando et al., 2009; Scambelluri et al., 2010; Deschamps et al., 2013; Gilotti,  
55 2013). However, the role played by the mantle wedge during (U)HP rock exhumation is still poorly  
56 understood. Some numerical models point to a negligible mantle involvement during exhumation  
57 (Yamato et al., 2008; Butler et al., 2013), whereas other models suggest that mantle rocks may be  
58 strongly involved, and may follow the exhumation path of buoyant (U)HP rocks towards the Earth's  
59 surface (Schwartz et al., 2001; Petersen and Buck, 2015). The behaviour of the mantle wedge  
60 during (U)HP rock exhumation may thus provide a key to discriminate among competing  
61 exhumation models (e.g., Agard et al. 2009; Guillot et al., 2009a; Liou et al., 2009; Warren, 2013).

62 In the Cenozoic metamorphic belt of the Western Alps, the geologic record of subduction and  
63 exhumation is exceptionally well preserved (e.g., Lardeaux et al., 2006; Malusà et al., 2011), but a  
64 high-resolution image of the mantle wedge is still lacking. A detailed analysis of the seismic  
65 velocity structure beneath the Dora-Maira (U)HP dome, where coesite attesting deep continental  
66 subduction was first described three decades ago (Chopin, 1984), may thus provide new insights on  
67 the ongoing debate concerning the mechanisms triggering the exhumation of (U)HP rocks (e.g.,  
68 Jolivet et al., 2003; Schwartz et al., 2001; Agard et al., 2009; Little et al., 2011; Butler et al., 2013;  
69 Malusà et al., 2015; Ducea, 2016). Moreover, this kind of analysis may provide new interpretation  
70 keys to understand the field relationships between mantle-wedge rocks and continental (U)HP rocks  
71 in deeply unroofed pre-Cenozoic orogenic belts (e.g., van Roermund, 2009; Scambelluri et al.,  
72 2010), where the geophysical record of subduction and exhumation is no longer preserved (e.g.,  
73 Zhao et al. 2017).

74 In this article, we exploit a comprehensive seismic dataset, also including anomalously deep  
75 earthquakes (Eva et al., 2015), to derive a local earthquake tomography model of the mantle wedge  
76 beneath the Dora-Maira (U)HP dome, which is then compared with the results provided by receiver  
77 function analysis along the CIFALPS transect (China-Italy-France Alps seismic survey; Zhao et al.,  
78 2015). Our results indicate that part of the mantle wedge was metasomatized above the Alpine  
79 subduction zone, and subsequently exhumed at shallow depth beneath continental (U)HP rocks now  
80 exposed at the surface. This suggests that mantle-wedge exhumation may be a prominent feature of  
81 the deep structure of many (U)HP belts, which should be integrated in future theoretical models of  
82 continental subduction and (U)HP rock exhumation.

## 83 **2. Tectonic framework**

### 84 ***2.1 The orogenic wedge of the southern Western Alps***

85 The Western Alps are the result of oblique subduction of the Alpine Tethys under the Adriatic  
86 microplate since the Late Cretaceous, followed by continental collision between the Adriatic and

87 European paleomargins during the Cenozoic (Coward and Dietrich, 1989; Dewey et al., 1989;  
88 Lardeaux et al., 2006; Handy et al. 2010; Malusà et al., 2016a). The resulting slab structure is still  
89 largely preserved (Zhao et al., 2016a), as well as the orogenic wedge formed atop the European slab  
90 (Lardeaux et al., 2006; Beltrando et al., 2010; Malusà et al., 2011). In the southern Western Alps,  
91 along the CIFALPS transect (X-X' in Fig. 1), the Alpine orogenic wedge mainly consists of rocks  
92 derived from the Piedmont ocean-continent transition and from the adjoining European paleomargin  
93 (Lemoine et al., 1986; Dumont et al., 2012). The external zone, exposed to the west of the Frontal  
94 Pennine Fault (FPF in Fig. 1), includes the Pelvoux and Argentera basements and their deformed  
95 Meso-Cenozoic sedimentary cover sequences (Ford et al., 2006), which record a transition from  
96 thin-skinned to thick-skinned compressional tectonics during the Neogene (Schwartz et al., 2017).  
97 East of the Frontal Pennine Fault, in the Alpine metamorphic wedge, the Briançonnais nappe stack  
98 (Br in Fig. 1) mainly consists of Upper Paleozoic to Mesozoic metasediments and underlying pre-  
99 Alpine basement rocks that underwent subduction starting from the Paleocene, and were later  
100 exhumed in the Eocene - early Oligocene (Malusà et al., 2002, 2005a; Ganne et al., 2007; Lanari et  
101 al., 2014). The Briançonnais nappe stack forms the core of the present-day Alpine fan-shaped  
102 structure (Michard et al., 2004) that was overprinted by a dense network of extensional faults during  
103 the Neogene (Sue et al., 2007; Malusà et al., 2009). The eastern part of the fan is formed by oceanic  
104 metasediments of the Schistes lustrés complex (SL in Fig. 1; Lemoine et al., 1986; Lagabrielle and  
105 Cannat, 1990), including boudinaged decametre-to-kilometre-sized ophiolitic bodies that were  
106 deformed and metamorphosed during Alpine subduction under blueschist to transitional blueschist-  
107 eclogite facies conditions (Agard et al., 2002; Tricart and Schwartz, 2006; Schwartz et al., 2009)  
108 (Fig. 2A). A ductile normal fault (DF1 in Fig. 2A; Ballèvre et al., 1990) separates the Schistes  
109 lustrés complex from the Viso metaophiolites (Vi in Fig. 1; Lombardo et al., 1978; Angiboust et al.,  
110 2012), representing major imbricated remnants of the Tethyan oceanic lithosphere that were  
111 deformed and metamorphosed under eclogite facies conditions during the Eocene (Duchêne et al.,  
112 1997; Schwartz et al., 2000; Rubatto and Hermann, 2003). Another ductile normal fault (DF2 in

113 Fig. 2A; Blake and Jayko, 1990) separates the Viso eclogites from the underlying stack of deeply  
114 subducted continental basement slices referred to as the Dora-Maira (U)HP dome (DM in Fig. 1;  
115 Henry et al., 1993; Michard et al., 1993), which also includes the coesite-bearing Brossasco-Isasca  
116 eclogitic unit (black star in Figs. 1 and 2A; Chopin et al., 1991; Compagnoni and Rolfo, 2003).  
117 Along the boundary with the Po Plain, the CIFALPS transect crosses the southern tip of the Lanzo  
118 massif (La in Fig. 1; Boudier, 1978; Piccardo et al., 2007), an eclogitized mantle slice separated  
119 from the Dora-Maira dome by a near-vertical active fault system rooted in the upper mantle (Rivoli-  
120 Marene deep fault - RMF in Fig. 1) at the southward prolongation of the Insubric Fault (Eva et al.  
121 2015; Malusà et al., 2017). The Lanzo massif consists of slightly serpentinized spinel plagioclase  
122 peridotites surrounded by a 3–5 km thick envelope of foliated serpentinites (Müntener et al., 2004;  
123 Debret et al., 2013), and records a high-pressure metamorphic peak of early Eocene age (Rubatto et  
124 al., 2008). Beneath the Po Plain, the complex transition zone between the Adriatic upper plate and  
125 the Apennines, also involving rotated fragments of the Alpine orogenic wedge (Maffione et al.,  
126 2008; Eva et al. 2015), is mainly covered by thick Cenozoic to Quaternary sedimentary successions.

## 127 ***2.2 The Dora-Maira (U)HP dome***

128 The Dora-Maira (U)HP dome is exposed all along the internal side of the southern Western  
129 Alps (Chopin et al., 1991; Lardeaux et al., 2006) (Fig. 1). To the west of Torino, it is juxtaposed  
130 against the Lanzo massif along the Lis-Trana deformation zone (Perrone et al., 2010), possibly  
131 representing a shallow splay of the Rivoli-Marene deep fault (Eva et al., 2015). To the south, it is  
132 partly buried by the sedimentary successions of the Po Plain (Fig. 1), and is exposed as a half-dome  
133 including coesite-bearing eclogitic rocks (Brossasco-Isasca unit) sandwiched between quartz-  
134 eclogite facies rocks, above, and blueschist facies rocks, below (Compagnoni et al. 1995; Avigad et  
135 al., 2003; Compagnoni and Rolfo, 2003) (Fig. 2A). The Brossasco-Isasca unit is a coherent  
136 continental crust sliver composed of granitic gneisses (Lenze and Stöckhert, 2007), whiteschists  
137 (Chen et al., 2017), mafic eclogites (Groppo et al., 2007) and impure marbles (Ferrando et al.,

138 2017). It was subducted to depths greater than ~100 km by the late Eocene (e.g., Chopin et al.,  
139 1991; Rubatto and Hermann, 2001; Hermann, 2003), and was exhumed close to the Earth's surface  
140 by the early Oligocene, at rates faster than subduction rates (Rubatto and Hermann, 2001; Malusà et  
141 al., 2015), as confirmed by low-temperature thermochronology data (Gebauer et al., 1997; Tricart et  
142 al., 2007; Beucher et al., 2012). The overlying quartz-eclogite Venasca *p.p.* and Dronero units,  
143 including gneisses and metasediments derived from a Permian-Triassic detrital sequence, and the  
144 underlying blueschist-facies Sanfront-Pinerolo unit, consisting of orthogneisses and metasediments  
145 intruded by Permian diorites (Avigad et al., 2003), were piled up together with the Brossasco-Isasca  
146 and Viso units during late Eocene exhumation (Schwartz et al., 2009; Malusà et al., 2011), to  
147 become part of the Eocene Eclogite belt now exposed along the upper-plate side of the Western  
148 Alps (Fig. 1), at the rear of a lower-pressure Paleogene wedge (LP in Fig. 2B,C).

149 The structure and lithologic composition of the orogenic wedge beneath the Dora-Maira  
150 (U)HP dome is still largely unknown. The velocity structure provided by available seismic  
151 tomography models is well resolved only for the uppermost 15-20 km (Paul et al., 2001; Béthoux  
152 et al., 2007). Recent tectonic reconstructions postulated the occurrence of Briançonnais crust  
153 slivers down to depths greater than 30 km, and suggested that these slivers would be involved in  
154 an east-vergent backfold at the scale of the whole Eclogite belt (Schmid et al., 2017). However,  
155 the Dora-Maira dome shows no cartographic evidence of such large-scale backfolding, which is  
156 instead observed in the Monte Rosa dome (MR in Fig. 1) of the northern Western Alps, where  
157 late backfolding is possibly ascribed to progressive westward shifting of Adria indentation from  
158 the Central Alps to the northern Western Alps during the Neogene (Malusà et al., 2016b). As a  
159 matter of fact, alternative interpretations of the deep tectonic structure of the southern Western  
160 Alps are not adequately supported by geophysical data. This information gap has so far precluded  
161 a full understanding of the exhumation mechanisms that were active within the Alpine subduction  
162 zone during the late Eocene.

### 163 *2.3 Exhumation models and implications on the deep orogenic structure*

164 In general terms, exhumation models applied to (U)HP belts can be framed within two different  
165 groups, also implying alternative scenarios of mantle involvement: (i) synconvergent exhumation  
166 models, either requiring fast erosion or forced circulation in a low-viscosity wedge (e.g., Beaumont  
167 et al., 2001; Zeitler et al., 2001; Jamieson and Beaumont, 2013), and (ii) exhumation models that  
168 consider boundary divergence within the subduction zone, with a minor role played by erosion (e.g.,  
169 Dewey, 1980; Brun and Faccenna, 2008). Both categories of models have been applied to the  
170 Western Alps (e.g., Malusà et al., 2011; Butler et al., 2013).

171 Classic tectonic reconstructions of the Alpine belt suggest that synconvergent exhumation  
172 could be favoured by deep duplex formation via the accretion of continental material derived from  
173 the lower plate (Schmid et al., 2004; Agard et al., 2009), which may be followed by indentation of  
174 the upper-plate mantle beneath the accretionary wedge (Schmid and Kissling, 2000; Béthoux et al.,  
175 2007). This scenario would imply that seismic velocities in the upper-plate mantle should be similar  
176 beneath the orogenic wedge and in the hinterland (Fig. 2B). In case of divergent motion between the  
177 upper plate and the descending slab, (U)HP rock exhumation might be instead associated to the  
178 emplacement of serpentinized mantle-wedge rocks at shallow depth beneath (U)HP continental  
179 rocks, provided that divergence is sufficiently high (Fig. 2C). Because of widespread mantle-wedge  
180 serpentinization during subduction (Lafay et al., 2013; Plümpner et al., 2017), seismic velocities are  
181 predicted to be lower in mantle-wedge rocks beneath the (U)HP dome, and higher in adjoining dry  
182 mantle rocks of the upper plate (Fig. 2C).

183 These alternative scenarios would be in agreement with alternative end-member tectonic  
184 reconstructions of the southern Western Alps, based on recent geophysical data from the CIFALPS  
185 experiment (Zhao et al., 2016b). One possible end-member reconstruction, consistent with  
186 geophysical data, invokes a thick complex of (U)HP continental slivers, in line with predictions of  
187 numerical models of syn-convergent exhumation, whereas a second end-member reconstruction  
188 invokes a larger volume of mantle rocks possibly exhumed at shallow depth during divergent



189 motion within the subduction zone (Zhao et al., 2015; Malusà et al., 2017). A local earthquake  
190 tomography model, complementing previous studies based on receiver function analysis, would be  
191 extremely useful to discriminate between these end-member tectonic reconstructions, and may  
192 allow a decisive step forward in our understanding of mechanisms leading to exhumation of (U)HP  
193 rocks.

### 194 **3. Methods**

#### 195 ***3.1. Building the database***

196 The local earthquake tomography presented in this work is largely based on the dataset collected  
197 during the CIFALPS experiment (Zhao et al., 2016b), which was integrated by data recorded in the  
198 same time interval by permanent seismic networks operating in Italy and France, and complemented  
199 with selected older events. The temporary network of the CIFALPS experiment (blue marks in  
200 Figure 1B) includes 46 broadband seismic stations deployed along a linear WSW-ESE transect  
201 from the European foreland to the western Po Plain, and 9 additional stations installed to the north  
202 and to the south of the main profile. Stations operated from July 2012 to September 2013, and were  
203 specifically deployed for a direct comparison between receiver function and local earthquake  
204 tomography. Stations located along the main profile were conceived for receiver function analysis  
205 (Zhao et al., 2015). Their spacing ranges from ~5 km in the Western Alps mountain range to ~10  
206 km in the European foreland and in the western Po Plain. Off profile stations were installed to  
207 improve the crossing of seismic rays for local earthquake tomography.

208 The high number of recording stations along the main CIFALPS profile may increase the  
209 computational burden during local earthquake tomography (e.g. in ray tracing) without a direct  
210 improvement in the final resolution. However, it ensures a number of advantages. For example, any  
211 potential loss of data due to station malfunctioning is easily recovered by adjacent instruments, and  
212 doubtful data can be discarded without jeopardizing the quality of the dataset. In order to improve  
213 the ray coverage and ensure ray crossing from any azimuth in the study volume, we added to the

214 dataset all published phase pickings recorded by permanent seismic stations operating in France and  
215 Italy during the CIFALPS experiment (red marks in Figure 1B). We additionally considered few  
216 events that occurred before the experiment to fill specific spatial gaps. This was the case of the  
217 intermediate depth earthquakes that were useful to sample anomalies at the bottom of the study  
218 volume. Because these earthquakes are relatively rare (Eva et al., 2015), only few events were  
219 recorded during the CIFALPS experiment. In summary, 270 events on a total of 1088 events  
220 utilized in this work were added as supplementary entries from datasets available at French and  
221 Italian seismic networks; about 80% of the remaining events were merged with existing phase  
222 pickings. The final P and S ray coverage is shown in Figure 3A.

### 223 ***3.2. Seismic tomography setup and reconstruction test***

224 We adopted the local earthquake tomography code SIMULPS (Thurber, 1983) for tomographic  
225 analysis, in its version 14 that implements the ray tracer by Virieux (1991) to cope with models of  
226 regional size. We subdivided the study volume into layers containing nodes, and used an initial  
227 velocity model derived from previous seismic experiments over a larger area (Scafidi et al., 2009).  
228 Several tests were performed for a correct choice of the inversion parameters, and classical damping  
229 trade-off curves (Eberhart-Phillips, 1986) were computed to pick up the best values for P and S  
230 velocities.

231 The resolution capability of the coupling between inversion setup and data was evaluated by  
232 checkerboard and reconstruction tests. These tests were useful to choose an adequate geometry of  
233 the starting model and evaluate the smearing due to the contrast between high and low velocity  
234 anomalies. The reconstruction test was specifically conceived to test the potential impact of the  
235 high-velocity Ivrea body, a long recognized tectonic feature associated to a positive gravimetric  
236 anomaly (red dotted line in Fig. 1) and interpreted as a slice of Adriatic mantle emplaced at shallow  
237 depth (Closs and Labrouste, 1963; Nicolas et al., 1990). We used a “stairwell” geometry to simulate  
238 a high-velocity east-dipping layer along the CIFALPS profile (Fig. 3B) and test the resolution

239 capability of the coupling between seismic dataset and inversion setup. The same geometry after  
240 interpolation by the algorithm used in SIMULPS is shown in Figure 3C. A comparison with Figure  
241 3B shows that the interpolation process introduces a smoothing of the anomalies and a band of fake  
242 colors around them. Figure 3D shows the reconstruction of the imposed stairwell structure based on  
243 our seismic dataset. The inversion of synthetic data does not consider the resolution, and Figure 3D  
244 only displays the reconstructed model as if it was completely resolved except for areas that were not  
245 sampled (in white). As shown in the reconstruction test, the shape of the anomaly is well  
246 reproduced, but the velocity of the first and second steps is lowered from  $\sim 8.0$  km/s (blueish) to  
247 about  $\sim 7.5$  km/s (greenish), and weak vertical and horizontal periodic stripes of yellow color appear  
248 at  $\sim 50$  km depth. These artifacts, and the underestimation of the magnitude of the high velocity  
249 anomalies in the uppermost 10 km of the crust, have been considered during the subsequent phases  
250 of tomography interpretation. The real data tomographic model is about  $700 \times 700$  km wide, and was  
251 obtained after 6 iterations on a 12 layers model of  $36 \times 36$  nodes each. In the central part of the  
252 model, spacing between nodes is equal to 15 km.

#### 253 **4. Results**

254 Figure 4 shows the  $V_p$  and  $V_p/V_s$  cross-sections along the CIFALPS profile. The lighter areas  
255 are those where the diagonal elements of the resolution matrix are  $< 0.1$ . This threshold was chosen  
256 as the divider between resolved and non-resolved areas based on a comprehensive comparisons  
257 between different resolution indicators (Paul et al., 2001). As expected, the maximum depth of the  
258 resolved area is limited by the depth of occurrence of most of the deepest events (Eva et al., 2015;  
259 Malusà et al., 2017). Beneath the Dora-Maira (U)HP dome, the tomography model is well resolved  
260 down to 50-60 km depth, whereas the two extremes of the CIFALPS cross section are poorly  
261 resolved. Letters “a” to “k” indicate the relevant velocity features highlighted by the tomography  
262 model. The main tectonic structures previously inferred from receiver function analysis (Zhao et al.

263 2015) and surface geology (Lardeaux et al., 2006; Malusà et al., 2015) are also indicated for  
264 comparison (black lines in Fig. 4).

265 The most prominent feature of the tomography model is represented by the high velocity body  
266 ( $V_p \sim 7.5$  km/s;  $V_p/V_s = 1.70$ - $1.72$ ), labelled with “a”, which is located right below the Dora-Maira  
267 (U)HP dome, at depths as shallow as  $\sim 10$  km. Such a high-velocity body was already imaged with  
268 similar velocities by previous works ( $V_p \sim 7.4$ - $7.7$  km/s; Paul et al., 2001; Béthoux et al., 2007), but  
269 was only resolved down to depths of 15-20 km. It is still observed to the south of the CIFALPS  
270 profile (Fig. 5D,E), but progressively vanishing towards the north (Fig. 5A,B). A series of N-S  
271 cross sections, ranging from the Western Alps to the Po Plain (Fig. 6), shows that this high-velocity  
272 anomaly is exclusively found beneath the Dora-Maira (U)HP dome (Fig. 6A), and disappears  
273 farther east.

274 The mantle-wedge region labelled with “b” is located at depth of 20-45 km, in correspondence  
275 with a cluster of intermediate depth earthquakes that mark the Rivoli-Marene deep fault (RMF in  
276 Fig. 4A; Eva et al., 2015). This region shows higher  $V_p$  values ( $\sim 8.0$  km/s) compared to region “a”,  
277 and anomalously high  $V_p/V_s$  ratios ( $> 1.74$ ) that are supportive of low shear wave velocities. This  
278 cluster of intermediate depth earthquakes in region “b” is not only observed along the CIFALPS  
279 profile, but also in cross sections located more to the north or to the south (Fig. 5). The deepest  
280 mantle wedge region resolved by the tomographic model is labelled with “c”. This region, located  
281 at depth of  $\sim 40$ - $50$  km atop the European slab, shows lower  $V_p$  and  $V_p/V_s$  values compared to  
282 region “b” ( $V_p \sim 7.0$ - $7.5$  km/s;  $V_p/V_s < 1.70$ ), but the  $V_p/V_s$  ratio is locally higher ( $V_p/V_s \sim 1.74$ ).

283 The well-resolved regions of the model also include some subducted European lower crust. This  
284 shows a progressive increase in  $V_p$  from the region labelled with “d” ( $V_p \sim 6.7$  km/s) to the region  
285 labelled with “e” ( $V_p \sim 7.6$  km/s), under a rather constant  $V_p/V_s$  ratio of 1.70-1.72. Such variations  
286 are detected in all of the analyzed WSW-ENE transects of Figure 5. No seismic event was recorded  
287 in regions “d” and “e” since 1990 (installation of permanent seismic networks) and during the  
288 CIFALPS experiment (Malusà et al., 2017).

289 On the eastern side of the transect, the region labelled with “f” is located below the Adriatic  
290 Moho as determined by receiver function analysis combined with gravity modelling. It shows Vp  
291 values ~8.0 km/s and Vp/Vs = 1.70-1.72. This region is affected by intermediate depth earthquakes  
292 that are also observed to the north and to the south of the CIFALPS transect (Fig. 5). The vertical  
293 and horizontal periodic stripes of yellow color observed at 50 km depth in this region are artifacts,  
294 as confirmed by the reconstruction test of Fig. 3D. Above the Adriatic Moho, measured Vp values  
295 are much lower, generally <6.7 km/s, but in places they reach values as high as ~7.2 km/s. Very  
296 high Vp/Vs values (>1.8) are locally observed at ~30 km depth at the base of the Adriatic crust.  
297 This region, labelled with “g”, is also characterized by a cluster of seismic events that are only  
298 observed in the vicinity of the main CIFALPS transect.

299 In the uppermost part of the Alpine orogenic wedge (regions “h” to “k”), Vp values are  
300 invariably <6.5 km/s, but major variations in Vp/Vs ratios are locally observed. For example, the  
301 region to the east of the Dora-Maira (U)HP dome (labelled with “h”) shows Vp/Vs values >1.72,  
302 whereas the region corresponding to the western flank of the Dora-Maira dome (labelled with “j”)  
303 shows much lower Vp/Vs ratios, even <1.66. Vp/Vs ratios <1.68 are also observed in the region  
304 labelled with “k”, located beneath the Frontal Pennine Fault. The double-vergence accretionary  
305 wedge located to the east of the Frontal Pennine Fault, and labelled with “i”, shows instead Vp/Vs  
306 values > 1.75, and includes most of the shallow earthquakes recorded in the Western Alps area.

## 307 **5. Comparison with receiver function analysis**

308 Results of local earthquake tomography are compared in Figure 7 with published CIFALPS  
309 results of receiver function analysis (Zhao et al., 2015). Unlike local earthquake tomography, the  
310 receiver function technique is based on the analysis of teleseismic earthquakes, and enhances P-to-S  
311 (Ps)-converted waves on velocity interfaces beneath an array. The polarity of the converted signal  
312 depends on the sign of the velocity change, and interfaces with velocity increase can be  
313 discriminated from interfaces with velocity decrease. Assumptions and arbitrary choices of the

314 receiver function approach applied to the CIFALPS transect (e.g., magnitude threshold, epicentral  
315 distance, seismograms filtering, velocity model, choice of the direction of back azimuths) are  
316 described in full in Zhao et al. (2015).

317 The image of Figure 7B is based on radial receiver functions from teleseismic events with  
318 magnitude  $\geq 5.5$ , epicentral distance of 30-90°, and ENE back-azimuths (see Zhao et al., 2015). This  
319 image shows two major interfaces marked by positive-polarity Ps-conversions (red-to-yellow  
320 regions), which attest the downward velocity increase corresponding to the European and Adriatic  
321 Mohos (thick dashed lines). The eastward-dipping European Moho is recognized from ~40 km  
322 depth beneath the Frontal Pennine Fault to ~75 km depth beneath the Po Plain. The Adriatic Moho  
323 is recognized from 20-30 km depth, to the east, to 10-15 km depth, to the west. The red spots  
324 located at 40-55 km depth beneath the Adriatic Moho are multiples, as confirmed by synthetic tests  
325 (Zhao et al., 2015). A shallow positive-polarity converted phase is also observed beneath the Dora-  
326 Maira massif, between regions “a” and “h”, whereas a spot of negative-polarity Ps-conversions  
327 marking a downward velocity decrease is located above region “c”, at 20-40 km depth (blue  
328 region).

329 On the eastern side of the CIFALPS transect, the sharp velocity increase from  $V_p < 6.5$  km/s to  
330  $V_p > 8$  km/s evidenced by local earthquake tomography faithfully matches the location of the  
331 downward velocity increase highlighted by receiver function analysis. Localized anomalies in  
332  $V_p/V_s$  ratios, e.g., in region “g”, match with major breaks in the alignment of positive-polarity Ps-  
333 conversions. Beneath the Dora-Maira (U)HP dome, the downward increase in  $V_p$  values from  
334 region “h” ( $V_p < 6.5$  km/s) to region “a” ( $V_p \sim 7.5$  km/s) is consistent with the observed positive-  
335 polarity Ps-conversions, whereas the downward velocity decrease from regions “a” and “b” ( $V_p$   
336  $\sim 7.5$  km/s and  $> 8$  km/s) to region “c” ( $V_p \sim 7.0-7.5$  km/s) is consistent with the spot of negative-  
337 polarity Ps-conversions located at 20-40 km depth in Figure 7B. The shape of the high-velocity  
338 region labelled with “a” is also mirrored by the distribution of seismic events recorded since 1990.  
339 Region “a” is virtually aseismic (Malusà et al., 2017), and earthquakes are chiefly located along its

340 external boundaries or in the surrounding regions (Fig. 7B). On the western side of the CIFALPS  
341 transect, the alignment of positive-polarity Ps-conversions generated along the European Moho is  
342 partly included within the resolved area of the local earthquake tomography model, and fits with a  
343 downward velocity increase from ~6.7 km/s (region “d”) to ~7.6 km/s (region “e”). The velocity  
344 structure unravelled by the analysis of local earthquakes is thus independently confirmed by the  
345 analysis of teleseismic earthquakes (Zhao et al., 2015) and by the distribution of seismic events  
346 (Eva et al., 2015; Malusà et al., 2017).

## 347 **6. Geologic interpretation**

348 The geologic cross section of Figure 7C shows the main features of the orogenic wedge of the  
349 Western Alps, and of the mantle wedge between the European and the Adriatic plates, as inferred  
350 from the velocity structure derived from local earthquake tomography along the CIFALPS profile.  
351 Correlation between seismic velocity and lithology in former subduction zones is a challenging  
352 task. Subducted rocks are heterogenous, and display anisotropic fabrics and velocity variations as a  
353 function of direction (e.g., Rudnick and Fountain, 1995; Weiss et al., 1999). A full 3D coverage of  
354 seismic rays is thus required to get a reliable characterization of the velocity structure (see Fig. 3A).

355 In the European plate, the  $V_p$  values ~6.7 km in region “d” are supportive of a relatively felsic  
356 composition of the European lower crust (e.g. Rudnick and Fountain 1995; Weiss et al., 1999;  
357 Goffé et al. 2003; Wang et al., 2005; Mechie et al. 2012). The homogeneous  $V_s$  values < 4 km/s  
358 reported by Lyu et al. (2017) suggest that the European lower crust may be rather homogeneous at  
359 the scale of seismic observations, and may consist of granulite having felsic to intermediate  
360 composition. Major occurrence of granulitic metapelites can be safely excluded, because it would  
361 result in much higher  $V_p$  (>6.7 km/s up to 7.2 km/s) and  $V_s$  values (~4 km/s; Rudnick and  
362 Fountain, 1995).

363 The increase in  $V_p$  values evidenced at ~40 km depth by local earthquake tomography, from  
364 ~6.7 km/s in region “d” to ~7.6 km/s in region “e”, may mirror a progressive eclogitization of lower

365 crust rocks with consequent density increase by metamorphic phase changes (e.g., Hacker et al.,  
366 2003; De Paoli et al., 2012). Mineral equilibria at the granulite-eclogite transition depend on rock  
367 composition. The eclogitization of a felsic granulite strongly increases the garnet content, and  
368 consequently the density from 2.90 to 3.30 kg/dm<sup>3</sup>, and the P velocity up to a maximum of 7.6 km/s  
369 (e.g., Christensen, 1989; Hacker et al., 2003, 2015; Hacker and Abers, 2004; Hetényi et al., 2007).  
370 These values are consistent with the V<sub>p</sub> values observed in region "e". The increase in P velocity  
371 from region "d" to region "e" is associated with a progressive increase in S velocity up to 4.2 km/s  
372 (Lyu et al., 2017), which may be either interpreted as an increase in mafic component, or as an  
373 effect of metamorphic reactions under increasing pressure-temperature conditions. However, V<sub>p</sub>  
374 values in region "e" are far too low for a pure mafic eclogite (Bezacier et al., 2010; Reynard, 2013),  
375 thus suggesting no major compositional changes from west to east in the European lower crust, but  
376 only a progressive change in metamorphic assemblage during subduction. This interpretation also  
377 explains the progressive weakening of the positive-polarity converted phases observed along the  
378 European Moho, from red to yellow background colours in Fig. 7B, as previously described by  
379 Zhao et al. (2015).

380 On the eastern side of the Western Alps, V<sub>p</sub> values >8 km/s confirm the presence of Adriatic  
381 mantle at shallow depth beneath the western Po Plain (10-15 km), just in correspondence with the  
382 positive gravimetric anomaly classically referred to as the Ivrea body (Closs and Labrouste, 1963;  
383 Nicolas et al., 1990) and in line with results of previous tomographic models (e.g., Solarino et al.,  
384 1997; Paul et al., 2001; Scafidi et al., 2006; 2009; Diehl et al., 2009; Wagner et al., 2012). East of  
385 the Ivrea body gravimetric anomaly, the Adriatic Moho is located at 30-35 km depth, which is a  
386 much more reliable estimate of the Moho depth beneath the Po Plain compared to previous  
387 estimates based on receiver function alone (Zhao et al., 2015). The locally high V<sub>p</sub>/V<sub>s</sub> ratios >1.8,  
388 associated to V<sub>p</sub> of 7.0-7.5 km/s (region "g"), may be supportive of gabbro (Weiss et al., 1999)  
389 underplated at the base of the Adriatic lower crust. Noteworthy, Permian gabbros are indeed  
390 exposed north of the Po plain, where they are intruded into lower crust rocks belonging to the



391 Adriatic (Southalpine) basement (Quick et al., 1994; Schaltegger and Brack, 2007). Above the  
392 Adriatic Moho, local spots with  $V_p \sim 7.2$  km/s but low  $V_p/V_s$  ratios (Fig. 5) are supportive of a  
393 more heterogeneous composition of the Adriatic lower crust compared to the European lower crust,  
394 and may suggest a local occurrence of granulite facies metapelites ( $V_p$  6.7-7.2 km/s,  $V_s \sim 4$  km/s;  
395 Rudnick and Fountain, 1995) not only at the surface (e.g., Ewing et al., 2014), but also at depth.  
396 Differences in velocity structure among crustal sections now exposed on the opposite sides of the  
397 Alps probably reflect a different pre-Alpine evolution, rather than processes related to the Cenozoic  
398 evolution of the Adria-Europe plate boundary zone (Guillot et al., 2009b; Carosi et al., 2012;  
399 Bergomi et al., in review).

400 In the uppermost part of the Alpine wedge, the structural variability of stacked rocks is largely  
401 mirrored by their variability in  $V_p/V_s$  ratios. The  $V_p/V_s$  values  $>1.75$  observed in the double-  
402 vergence accretionary wedge chiefly including Briançonnais and Schistes lustrés units (Lardeaux et  
403 al., 2006), may reflect low  $V_s$  values, possibly associated to the widespread network of mesoscale  
404 faults developed in these rocks since the Neogene (Tricart et al., 2004; Sue et al., 2007; Malusà et  
405 al., 2009). To the east, low  $V_p/V_s$  values even  $<1.66$  observed on the western flank of the Dora-  
406 Maira dome (region “j”) may instead reflect high  $V_s$  velocities, suggesting that the poorly fractured  
407 granitic gneisses exposed at the surface (Brossasco granite; Paquette et al., 1999; Lenze and  
408 Stöckhert, 2007) may be also present at depth. Fracturing may be also invoked to explain the low  
409  $V_s$  values observed along the eastern boundary of the Dora-Maira dome, where (U)HP continental  
410 rocks are juxtaposed against the eclogitized mantle rocks of the Lanzo massif (Kienast and  
411 Pognante, 1988; Piccardo et al., 2007) along the Lis-Trana deformation zone (Perrone et al., 2010).  
412 To the west of the Frontal Pennine Fault,  $V_p/V_s$  values  $<1.68$  suggest instead that the European  
413 upper crust in the External zones is poorly deformed, consistent with minor seismicity recorded in  
414 that area (Fig. 7B).

415 But the most relevant results of the tomography model presented in this work is related to the  
416 velocity structure beneath the Dora-Maira (U)HP dome. This information is critical to discriminate

417 between contrasting models of (U)HP rock exhumation (Malusà et al., 2011, 2015; Jamieson and  
418 Beaumont, 2013), and to discern between end-member tectonic reconstructions recently proposed in  
419 the light of available geophysical data (Malusà et al., 2017). The velocity structure of the mantle  
420 wedge region “a”, showing Vp velocity of ~7.5 km/s from depths as shallow as ~10 km down to  
421 ~30 km, is largely inconsistent with the presence of imbricated continental crust units (e.g., Schmid  
422 et al., 2017) or dry mantle peridotite beneath the Dora-Maira (U)HP dome. Instead, it may suggest a  
423 complex evolution of mantle-wedge rocks in terms of P-T conditions and fluid-rock interaction.  
424 Such Vp values point in fact to widespread serpentinization of mantle rocks (~60% according to  
425 Reynard, 2013), that may locally exceed 90% both in the uppermost part of anomaly “a” and in the  
426 Lanzo massif, although velocity values in the uppermost crustal levels may be slightly  
427 underestimated, as unravelled by the reconstruction tests of Fig. 3D. The degree of serpentinization  
428 at 30-40 km depth is instead much lower (<30%), and consistent with the occurrence of  
429 intermediate-depth earthquakes (Fig. 7B). Vp/Vs ratios are in the range of 1.70-1.72 in region “a”,  
430 but sharply increase to values >1.74 in region “b”, where Vp values (~8.0 km/s) are consistent with  
431 dry mantle peridotite. The high Vp/Vs ratios in region “b” point to low shear wave velocities, which  
432 are in line with a potential impact of the Rivoli-Marene deep fault on the rock fabric. According to  
433 previous work, the deepest part of the mantle wedge beneath the thick blue spot of negative polarity  
434 conversions (region “c” in Fig. 7B) may either include serpentinites, or slivers of (U)HP rocks. On a  
435 geophysical ground, serpentinites can be easily distinguished from other lithologies possibly found  
436 in high-pressure mélange zones (e.g., Marschall and Schumacher, 2012) such as eclogitic  
437 metasediments and mafic eclogites (Reynard, 2013). Our results indicate that the velocity values  
438 observed in region “c” (Vp ~7.0-7.5 km/s; Vp/Vs <1.70) are neither consistent with eclogitic  
439 metasediments (Vp ~7.0 km/s; Vp/Vs ~1.75) nor with mafic eclogite (Vp > 8.0 Vp/Vs ~1.73), but  
440 are instead supportive of ultramafic rocks with a degree of serpentinization ranging between 50%  
441 and 75% (Weiss et al., 1999; Reynard, 2013). However, minor slivers of eclogitic metasediments

442 could be present at ~40 km depth at the top of the European slab, in regions showing the highest  
443  $V_p/V_s$  ratios (Fig. 7A).

#### 444 **7. Implication for (U)HP rock exhumation**

445 In the southern Western Alps, the positive gravimetric anomaly ascribed to the Ivrea body is  
446 classically interpreted in terms of upper mantle indentation (e.g., Lardeaux et al., 2006; Béthoux et  
447 al., 2007), in line with previous tectonic interpretations proposed for the Central Alps and for the  
448 northern Western Alps (e.g., Schmid and Kissling, 2000). According to these interpretations, the  
449 uppermost part of the Adriatic mantle would act as an indenter beneath the Alpine accretionary  
450 wedge, and would transfer compression towards the European foreland. The main geologic  
451 implications of this model include major crustal shortening in the upper plate, and fast erosion  
452 focused above the indenter (Fig. 2B). These latter features are indeed observed in the Central Alps,  
453 where upper mantle indentation, accommodated by back-folding of (U)HP domes (Keller et al.,  
454 2005) and by backthrusting of Adriatic units (Zanchetta et al., 2015), triggered the fast erosional  
455 exhumation of the amphibolite-facies rocks of the Lepontine dome (Anfinson et al., 2016; Malusà et  
456 al., 2016b). However, these features are not common to the southern Western Alps, where  
457 shortening in the accretionary wedge was minor during and after (U)HP rock exhumation (Malusà  
458 et al., 2009; Dumont et al., 2012), and erosion was much slower compared to the Lepontine dome,  
459 as attested by low-temperature thermochronometers (Malusà et al., 2005b; Vernon et al., 2008; Fox  
460 et al., 2015) and by preserved Oligocene corals unconformably lying on top of Eocene eclogites  
461 (Molare Fm; Quaranta et al. 2009). A tectonic scenario exclusively invoking upper-plate mantle  
462 indentation beneath the accretionary wedge would also imply that seismic velocities in the upper-  
463 plate mantle should be quite similar beneath the orogenic wedge and in the hinterland (Fig. 2B).  
464 Major seismic velocity changes, e.g., by metamorphic phase changes triggered by fluids released by  
465 the downgoing slab, would remain undetected in local earthquake tomography models, because they  
466 would take place at much greater depths (Deschamps et al., 2013; Abers et al., 2017).

467 Our study points to a complex velocity structure in the upper-plate mantle of the southern  
468 Western Alps. The region beneath the Dora-Maira (U)HP dome is dominated by serpentinitized  
469 peridotites, documented from ~10 km depth down to the top of the European slab. To the east, these  
470 rocks are juxtaposed against dry mantle peridotites of the Adriatic upper plate along a steeply  
471 dipping fault rooted in the lithospheric mantle (RMF in Fig. 7C). In between, mantle rocks of the  
472 Lanzo massif underwent subduction during the Alpine orogeny, and were later exhumed and  
473 accreted against the Adriatic upper plate when the Dora-Maira (U)HP rocks were still buried at  
474 mantle depths (Rubatto and Hermann, 2001). This scenario is supportive of (U)HP rock and mantle-  
475 wedge exhumation triggered by upper plate divergent motion (Fig. 2C).

476 Serpentinitized peridotites with  $V_p \sim 7.5$  km/s that are found beneath the Dora-Maira dome may  
477 have favoured the exhumation of (U)HP rocks across the upper crust, in the depth range where  
478 eclogitized continental crust rocks may have become neutrally buoyant (Schwartz et al., 2001).  
479 According to Agard et al. (2009), exhumation of eclogitized ophiolites would be favoured by  
480 accretion of continental material. Our results point instead to a decisive role played by buoyant  
481 serpentinites (e.g., Hermann et al., 2000; Schwartz et al., 2001) during continental (U)HP rock  
482 exhumation, within a broadly extensional tectonic framework that is common to many recent  
483 tectonic reconstructions of the Central Mediterranean area (e.g., Vignaroli et al., 2008; Malusà et  
484 al., 2015) (Fig. 8).

485 No exhumed mantle-wedge serpentinites are recognized so far at outcrop in the southern  
486 Western Alps (Scambelluri et al., 1995; Piccardo et al., 2004; Hattori and Guillot, 2007; Deschamps  
487 et al., 2013). However strong fluid-rock interactions are recognized in subducted serpentinites and  
488 associated ophiolitic rocks (Scambelluri and Tonarini, 2012; Lafay et al., 2013; Plümper et al.,  
489 2017), suggesting that fluid release may have occurred during oceanic and even during continental  
490 subduction (e.g., Castelli et al., 2007; Ferrando et al., 2009), possibly triggering the partial  
491 serpentinitization of the Adriatic mantle wedge. Part of the Adriatic mantle wedge was then exhumed  
492 at shallow crustal levels during late Eocene transtension along the Western Alps subduction zone

493 (Malusà et al., 2015) and coeval rapid exhumation of the Dora-Maira (U)HP rocks (Rubatto and  
494 Hermann, 2001) (step 1 in Fig. 8). The exhumed mantle wedge was finally indented beneath the  
495 Alpine belt during early Oligocene tectonic shortening (Dumont et al., 2012; Jourdan et al., 2012,  
496 2013) (step 2 in Fig. 8). Along the Adria-Europe plate boundary, the divergent component of  
497 Eocene transtension progressively decreased towards the north to become negligible in the Central  
498 Alps (Fig. 8A), where Adria was indented more deeply beneath the accretionary wedge compared to  
499 the Western Alps, and rocks now exposed in the Lepontine dome were exhumed at lower rates  
500 through the upper crust (Fig. 8B). We speculate that, north of the Dora-Maira dome, upper plate  
501 divergence was probably insufficient to allow an effective exhumation of the mantle wedge (Fig.  
502 8C). However, testing this hypothesis would require a high resolution tomographic image of the  
503 northern Western Alps, which may be precluded by the lack of deep earthquakes.

504 Our results demonstrate that recent geologic cross-sections postulating a thick wedge of  
505 Briançonnais eclogites beneath the Dora-Maira dome (e.g., Schmid et al., 2017) are likely incorrect.  
506 The palinspastic reconstructions derived from such geologic cross-sections, and exclusively  
507 considering a Cenozoic evolution within a broadly compressional framework, should be  
508 reconsidered at the advantage of palinspastic reconstructions also including major episodes of  
509 divergence within the plate boundary zone (e.g., Vignaroli et al., 2008; Malusà et al., 2015). Mantle  
510 wedge exhumation is in fact more consistent with a late Eocene transtensional tectonic framework  
511 (Fig. 8C) followed by early Oligocene convergence (Fig. 8D), accommodated by orogen-  
512 perpendicular shortening in the external Alps (Dumont et al., 2012) and by transpressional tectonics  
513 in the Alps-Appennines transition zone (Malusà and Balestrieri, 2012).

514 The occurrence of mantle-wedge serpentinites exhumed at shallow depth within a continental  
515 subduction zone is not specific of the southern Western Alps. Mantle wedge serpentinites associated  
516 with (U)HP rock are described, for example, in the Indus Suture Zone in the Himalaya, in the  
517 Carribean (Guillot et al., 2001; Deschamps et al., 2012), in the Western Gneiss Region in Norway  
518 (Scambelluri et al., 2010), and are inferred by geophysical evidence under the Dabie-Sulu (Liu et

519 al., 2015). Our findings suggest that orogen-scale exhumation of the mantle wedge may represent a  
520 prominent, but still underestimated feature of the deep structure of many orogenic belts. As such, it  
521 should be integrated in more advanced theoretical models of subduction and exhumation. Moreover,  
522 widespread mantle-wedge exhumation may explain the common occurrence of boudinaged mantle-  
523 wedge rocks within continental UHP rocks in the roots of old orogenic belts now unroofed by  
524 erosion. In pre-Cenozoic orogenic belts such as the Dabie-Sulu or the Western Gneiss Region,  
525 where the evidence of minor erosion during UHP exhumation, if any, is no longer preserved, the  
526 occurrence of mantle wedge rocks at shallow depth may represent the only evidence supporting  
527 (U)HP rock exhumation triggered by divergent motion between upper plate and accretionary  
528 wedge.

## 529 **8. Conclusions**

530 The new local earthquake tomography model of the southern Western Alps, independently  
531 validated by receiver function analysis, unravels a complex seismic velocity pattern consistent with  
532 a composite structure of the mantle wedge above the subducted European lithosphere. Seismic  
533 velocities indicate that the Dora-Maira (U)HP dome lays directly above serpentinitized peridotites,  
534 documented from ~10 km depth down to the top of the eclogitized lower crust of the European  
535 plate. We propose that peridotite serpentinitization was the result of fluids released to the Adriatic  
536 mantle wedge during Alpine subduction. During late Eocene transtension, when the subduction  
537 wedge was largely exhumed at the Earth's surface, part of the mantle wedge was also exhumed at  
538 shallow crustal levels, to be finally indented under the Alpine metamorphic units in the early  
539 Oligocene. Our results suggest that mantle wedge exhumation may represent an important feature of  
540 the deep structure of exhumed continental subduction zones. Deep orogenic levels, as those imaged  
541 by local earthquake tomography in the southern Western Alps, may be exposed today in older  
542 continental subduction zones, where mantle wedge serpentinites are commonly associated to  
543 continental (U)HP metamorphic rocks.

544 **Acknowledgments.** This work is funded by the State Key Laboratory of Lithospheric Evolution, China, the National  
545 Natural Science Foundation of China (Grant 41350001), and a grant from LabEx OSUG@2020 (Investissements  
546 d'avenir; ANR10 LABX56, France). The earthquake waveforms used in this study are available at the European  
547 Integrated Data Archive (eida.rm.ingv.it) (see also doi:10.13127/SD/X0FXnH7QfY; doi:10.12686/sed/networks/2a).  
548 The CIFALPS seismic data are archived at the data center of the Seismic Array Laboratory, Institute of Geology and  
549 Geophysics, Chinese Academy of Sciences, and at the data center of the French Seismologic and Geodetic Network  
550 RESIF (doi:10.15778/RESIF.YP2012). The manuscript benefited from constructive reviews by F. Rossetti and an  
551 anonymous reviewer, comments by M. Scambelluri, and insightful discussions with S. Baldwin, S. Ferrando and N.  
552 Malaspina.

## 553 **References**

- 554 Abers, G. A., van Keken, P. E., Hacker, B. R., 2017. The cold and relatively dry nature of mantle forearcs in  
555 subduction zones. *Nature Geoscience* 10(5), 333-337.
- 556 Agard, P., Monie, P., Jolivet, L., Goffé, B., 2002. Exhumation of the Schistes Lustrés complex: In situ laser  
557 probe Ar-40/Ar-39 constraints and implications for the western Alps. *Journal of Metamorphic*  
558 *Geology* 20, 599–618.
- 559 Agard, P., Yamato, P., Jolivet, L., Burov, E., 2009. Exhumation of oceanic blueschists and eclogites in  
560 subduction zones: timing and mechanisms. *Earth-Science Reviews* 92(1), 53-79.
- 561 Angiboust, S., Langdon, R., Agard, P., Waters, D. J., Chopin, C. 2012. Eclogitization of the Monviso ophiolite  
562 (W Alps) and implications on subduction dynamics. *Journal of Metamorphic Geology* 30, 37–61.
- 563 Avigad, D., Chopin, C., Le Bayon, R., 2003. Thrusting and extension in the southern Dora-Maira ultra-high-  
564 pressure massif (Western Alps): view from below the coesite-bearing unit. *The Journal of geology*  
565 111(1), 57-70.
- 566 Ballèvre, M., Lagabrielle, Y., Merle, O., 1990. Tertiary ductile normal faulting as a consequence of  
567 lithospheric stacking in the western Alps. *Société Géologique de France, Mémoires* 156, 227–236.
- 568 Beaumont, C., Jamieson, R.A., Nguyen, M.H., Lee, B., 2001. Himalayan tectonics explained by extrusion of  
569 a low-viscosity crustal channel coupled to focused surface denudation. *Nature* 414, 738-742.
- 570 Becker, H., 1993. Garnet peridotite and eclogite Sm-Nd mineral ages from the Lepontine dome (Swiss Alps):  
571 New evidence for Eocene high-pressure metamorphism in the central Alps. *Geology* 21, 599-602.
- 572 Beltrando, M., Compagnoni, R., Lombardo, B., 2010. (Ultra-) High-pressure metamorphism and orogenesis:  
573 An Alpine perspective. *Gondwana Research* 18(1), 147-166.
- 574 Bergomi, M.A., Dal Piaz, G.V., Malusà M.G., Monopoli, B., Tunesi, A. The Grand St Bernard -  
575 Briançonnais nappe system and the Paleozoic inheritance of the Western Alps unravelled by zircon U-  
576 Pb dating. *Tectonics* (in review).
- 577 Béthoux, N., Sue, C., Paul, A., Virieux, J., Fréchet, J., Thouvenot, F., Cattaneo, M., 2007. Local tomography  
578 and focal mechanisms in the south-western Alps: comparison of methods and tectonic implications.  
579 *Tectonophysics* 432, 1–19.
- 580 Beucher, R., van der Beek, P., Braun, J., Batt, G. E., 2012. Exhumation and relief development in the  
581 Pelvoux and Dora-Maira massifs (western Alps) assessed by spectral analysis and inversion of  
582 thermochronological age transects. *Journal of Geophysical Research: Earth Surface*, 117(F3).

- 583 Bezacier, L., Reynard, B., Bass, J.D., Wang, J., Mainprice, D., 2010. Elasticity of glaucophane, seismic  
584 velocities and anisotropy of the subducted oceanic crust. *Tectonophysics* 494, 201–210.
- 585 Blake, M.C., Jayko, A.S., 1990. Uplift of very high pressure rocks in the western Alps: Evidence for  
586 structural attenuation along low angle faults. In: Roure, F., Heitzmann, P., Polino, R. (Eds.), *Deep*  
587 *structure of the Alps. Mémoire de la Société Géologique de France* 156, pp. 228–237.
- 588 Boudier, F., 1978. Structure and petrology of the Lanzo peridotite massif (Piedmont Alps). *Geological*  
589 *Society of America Bulletin* 89(10), 1574-1591.
- 590 Brouwer, F.M., van de Zedde, D.M.A., Wortel, M.J.R., Vissers, R.L.M., 2004. Late-orogenic heating during  
591 exhumation: Alpine PTt trajectories and thermomechanical models. *Earth and Planetary Science*  
592 *Letters* 220, 185-199.
- 593 Brun, J. P., Faccenna, C., 2008. Exhumation of high-pressure rocks driven by slab rollback. *Earth and*  
594 *Planetary Science Letters* 272(1), 1-7.
- 595 Butler, J.P., Beaumont, C., Jamieson, R.A., 2013. The Alps 1: A working geodynamic model for burial and  
596 exhumation of (ultra) high-pressure rocks in Alpine-type orogens. *Earth and Planetary Science Letters*  
597 377, 114–131.
- 598 Carosi, R., Montomoli, C., Tiepolo, M., Frassi, C., 2012. Geochronological constraints on post-collisional  
599 shear zones in the Variscides of Sardinia (Italy). *Terra Nova* 24(1), 42-51.
- 600 Carswell, D. A., R. Compagnoni (Eds.), 2003. *Ultrahigh Pressure Metamorphism*, 508 pp., Eotvos Univ.  
601 Press, Budapest.
- 602 Castelli, D., Rolfo, F., Groppo, C., Compagnoni, R., 2007. Impure marbles from the UHP Brossasco-Isasca  
603 Unit (Dora-Maira Massif, western Alps): evidence for Alpine equilibration in the diamond stability  
604 field and evaluation of the X(CO<sub>2</sub>) fluid evolution *Journal of Metamorphic Geology*, 25, 587-603
- 605 Chen, Y. X., Zhou, K., Zheng, Y. F., Schertl, H. P., 2017. Zircon geochemical constraints on the protolith  
606 nature and metasomatic process of the Mg-rich whiteschist from the Western Alps. *Chemical Geology*  
607 467, 177-195.
- 608 Chopin, C., 1984. Coesite and pure pyrope in high-grade blueschists of the Western Alps: A first record and  
609 some consequences. *Contributions to Mineralogy and Petrology* 86, 107–118.
- 610 Chopin, C., Henry, C., Michard, A., 1991. Geology and petrology of the coesite bearing terrain, Dora-Maira  
611 massif, western Alps. *European Journal of Mineralogy* 3, 263–291.
- 612 Christensen, N.I., 1989. Seismic velocities. In: Carmichael, R.S. (Ed.), *Practical Handbook of Physical*  
613 *Properties of Rocks and Minerals*. CRC Press, Boca Raton, p. 741.
- 614 Closs, H. and Labrouste Y. (Eds.), 1963. *Recherches séismologiques dans les Alpes occidentales au moyen*  
615 *de grandes explosions en 1956, 1958 et 1960. Mem. Coll. Année Geophys. Int.* 12-2. CNRS Paris, 241  
616 pp.
- 617 Compagnoni, R., Hirajima, T., Chopin, C., 1995. Ultra-high-pressure metamorphic rocks in the Western  
618 Alps. In: Coleman, R.G., Wang, X. (Eds.), *Ultrahigh Pressure Metamorphism*. Cambridge University  
619 Press, Cambridge, UK, pp. 206–243.
- 620 Compagnoni, R., Rolfo, F., 2003. UHPM units in the western Alps: *European Mineralogy Union Notes in*  
621 *Mineralogy* 5, 13–49.
- 622 Coward, M., Dietrich, D., 1989. Alpine tectonics: an overview. In: Coward, M., Dietrich, D., Park, R.G.  
623 (Eds), *Alpine Tectonics*. Geological Society, London, Special Publications 45, pp. 1–29.
- 624 De Paoli, M. C., Clarke, G. L., Daczko, N. R., 2012. Mineral equilibria modeling of the granulite–eclogite  
625 transition: effects of whole-rock composition on metamorphic facies type-assemblages. *Journal of*  
626 *Petrology* 53(5), 949-970.
- 627 Debret, B., Nicollet, C., Andreani, M., Schwartz, S., Godard, M., 2013. Three steps of serpentinitization in an  
628 eclogitised oceanic serpentinitisation front (Lanzo massif - Western Alps). *Journal of Metamorphic*  
629 *Geology* 31, 165–186.



- 630 Deschamps, F., Godard, M., Guillot, S., Chauvel, C., Andreani, M., Hattori K., Wunder B., France L., 2012.  
631 Behavior of fluid-mobile elements in serpentines from abyssal to subduction environments: Examples  
632 from Cuba and Dominican Republic. *Chemical Geology* 313, 93–117.
- 633 Deschamps, F., Godard, M., Guillot, S., Hattori, K.H., 2013. Geochemistry of subduction zone serpentinites:  
634 A review. *Lithos* 178, 96-127.
- 635 Dewey, J.F., 1980. Episodicity, sequence and style at convergent plate boundaries. *Geological Association  
636 of Canada Special Paper* 2, 553-576.
- 637 Dewey, J. F., Helman, M. L., Knott, S. D., Turco, E., Hutton, D. H. W. (1989). Kinematics of the western  
638 Mediterranean. *Geological Society, London, Special Publications* 45(1), 265-283.
- 639 Diehl, T., Husen, S., Kissling, E., Deichmann, N., 2009. High-resolution 3-D P-wave model of the Alpine  
640 crust. *Geophysical Journal International* 179(2), 1133–1147.
- 641 Ducea, M. N., 2016. Research Focus: Understanding continental subduction: A work in progress. *Geology*  
642 44, 239-240.
- 643 Duchêne, S., Blichert-Toft, J., Luais, B., Télouk, P., Lardeaux, J.M., and Albarède, F., 1997. The Lu-Hf  
644 dating of garnets and the ages of the Alpine high-pressure metamorphism. *Nature* 387, 586–589.
- 645 Dumont, T., Schwartz, S., Guillot, S., Simon-Labric, T., Tricart, P., Jourdan, S., 2012. Structural and sedimentary  
646 records of the Oligocene revolution in the Western Alps. *Journal of Geodynamics* 56, 18–38.
- 647 Eberhart-Phillips, D., 1986. Three-dimensional velocity structure in northern California Coast Ranges from  
648 inversion of local earthquake arrival times. *Bulletin of the Seismological Society of America* 76(4),  
649 1025–1052.
- 650 Eva, E., Malusà, M.G., Solarino, S., 2015. A seismotectonic picture of the inner southern Western Alps  
651 based on the analysis of anomalously deep earthquakes. *Tectonophysics* 661, 190–199.
- 652 Ewing, T. A., Rubatto, D., Hermann, J., 2014. Hafnium isotopes and Zr/Hf of rutile and zircon from lower  
653 crustal metapelites (Ivrea–Verbanò Zone, Italy): implications for chemical differentiation of the crust.  
654 *Earth and Planetary Science Letters* 389, 106-118.
- 655 Ferrando, S., Frezzotti, M. L., Petrelli, M., Compagnoni, R., 2009. Metasomatism of continental crust during  
656 subduction: the UHP whiteschists from the Southern Dora-Maira Massif (Italian Western Alps).  
657 *Journal of Metamorphic Geology* 27(9), 739-756.
- 658 Ferrando, S., Groppo, C., Frezzotti, M. L., Castelli, D., Proyer, A., 2017. Dissolving dolomite in a stable  
659 UHP mineral assemblage: Evidence from Cal-Dol marbles of the Dora-Maira Massif (Italian Western  
660 Alps). *American Mineralogist* 102(1), 42-60.
- 661 Ford, M., Duchêne, S., Gasquet, D., Vanderhaeghe, O., 2006. Two-phase orogenic convergence in the  
662 external and internal SW Alps. *Journal of the Geological Society* 163, 815–826.
- 663 Fox, M., Herman, F., Kissling, E., Willett, S.D., 2015, Rapid exhumation in the Western Alps driven by slab  
664 detachment and glacial erosion. *Geology*, 43, 379–382.
- 665 Ganne, J., Bertrand, J.M., Fudral, S., Marquer, D., Vidal, O., 2007. Structural and metamorphic evolution of  
666 the Ambin massif (western Alps): toward a new alternative exhumation model for the Briançonnais  
667 domain. *Bulletin de la Société Géologique de France* 178, 437–458.
- 668 Gebauer, D., 1996. A P-T-t path for an (ultra?-) high-pressure ultramafic/mafic rock-association and its felsic  
669 country-rocks based on SHRIMP-dating of magmatic and metamorphic zircon domains. Example:  
670 Alpe Arami (Central Swiss Alps), in: Basu, A., Hart, S. (Eds.), *Earth Processes: Reading the Isotopic  
671 Code*. *Geophys. Monograph* 95, Am. Geophys. Union, Washington, DC, pp. 307-330.
- 672 Gebauer, D. H. P. S., Schertl, H. P., Brix, M., Schreyer, W., 1997. 35 Ma old ultrahigh-pressure  
673 metamorphism and evidence for very rapid exhumation in the Dora Maira Massif, Western Alps.  
674 *Lithos* 41, 5-24.
- 675 Gilotti, J. A., 2013. The realm of ultrahigh-pressure metamorphism. *Elements* 9, 255–260.

- 676 Goffé, B., Bousquet, R., Henry, P., Le Pichon, X., 2003. Effect of the chemical composition of the crust on  
677 the metamorphic evolution of orogenic wedges. *Journal of metamorphic geology* 21(2), 123-141.
- 678 Groppo, C., Lombardo, B., Castelli, D., Compagnoni, R., 2007. Exhumation history of the UHPM  
679 Brossasco-Isasca Unit, Dora-Maira Massif, as inferred from a phengite-amphibole eclogite.  
680 *International Geology Review* 49(2), 142-168.
- 681 Guillot, S., Hattori, K.H., de Sigoyer, J., Nägler, T., Auzende, A.L., 2001. Evidence of hydration of the mantle  
682 wedge and its role in the exhumation of eclogites. *Earth and Planetary Science Letters* 193, 115–127.
- 683 Guillot, S., Hattori, K., Agard, P., Schwartz, S., Vidal, O., 2009a. Exhumation Processes in Oceanic and  
684 Continental Subduction Contexts: A Review, Springer, Berlin.
- 685 Guillot, S., di Paola, S., Ménot, R. P., Ledru, P., Spalla, M. I., Gosso, G., Schwartz, S., 2009b. Suture zones  
686 and importance of strike-slip faulting for Variscan geodynamic reconstructions of the External  
687 Crystalline Massifs of the western Alps. *Bulletin de la Société Géologique de France* 180(6), 483-500.
- 688 Hacker, B. R., Abers, G. A., 2004. Subduction Factory 3: An Excel worksheet and macro for calculating the  
689 densities, seismic wave speeds, and H<sub>2</sub>O contents of minerals and rocks at pressure and temperature.  
690 *Geochemistry, Geophysics, Geosystems* 5(1).
- 691 Hacker, B.R., Abers, G.A., Peacock, S.M., 2003. Subduction factory 1. Theoretical mineralogy, densities,  
692 seismic wave speeds, and H<sub>2</sub>O contents. *Journal of Geophysical Research: Solid Earth* 108 (B1).
- 693 Hacker, B.R., McClelland, W.C., Liou J.G. (Eds.), 2006. Ultrahigh-pressure metamorphism: Deep  
694 continental subduction, Special Paper Geological Society of America 403, 206 pp.
- 695 Hacker, B. R., Kelemen, P. B., Behn, M. D., 2015. Continental lower crust. *Annual Review of Earth and*  
696 *Planetary Sciences* 43, 167-205.
- 697 Handy, M.R., Schmid, S.M., Bousquet, R., Kissling, E., Bernoulli, D., 2010. Reconciling plate-tectonic  
698 reconstructions of Alpine Tethys with the geological–geophysical record of spreading and subduction  
699 in the Alps. *Earth-Science Reviews* 102(3), 121-158.
- 700 Hattori, K.H., Guillot, S., 2007. Geochemical character of serpentinites associated with high- to ultrahigh-  
701 pressure metamorphic rocks in the Alps, Cuba, and the Himalayas: Recycling of elements in  
702 subduction zones, *Geochemistry, Geophysics, Geosystems* 8, Q09010, doi:10.1029/2007GC001594.
- 703 Henry, C., Michard, A., Chopin, C., 1993. Geometry and structural evolution of ultra-high pressure and high-  
704 pressure rocks from the Dora-Maira massif, western Alps, Italy. *Journal of Structural Geology* 15,  
705 965–981.
- 706 Hermann, J., 2003. Experimental evidence for diamond-facies metamorphism in the Dora-Maira massif.  
707 *Lithos* 70(3), 163-182.
- 708 Hermann, J., Müntener, O., Scambelluri, M., 2000. The importance of serpentinite mylonites for subduction  
709 and exhumation of oceanic crust. *Tectonophysics* 327(3), 225-238.
- 710 Hetényi, G., Cattin, R., Brunet, F., Bollinger, L., Vergne, J., Nábělek, J. L., Diament, M., 2007). Density  
711 distribution of the India plate beneath the Tibetan plateau: Geophysical and petrological constraints on  
712 the kinetics of lower-crustal eclogitization. *Earth and Planetary Science Letters* 264(1), 226-244.
- 713 Jamieson, R.A., Beaumont, C., 2013. On the origin of orogens. *Geological Society of America Bulletin*  
714 125(11-12), 1671–1702.
- 715 Jolivet, L., Faccenna, C., Goffé, B., Burov, E., Agard, P., 2003. Subduction tectonics and exhumation of  
716 high-pressure metamorphic rocks in the Mediterranean orogens. *American Journal of Science* 303(5),  
717 353-409.
- 718 Jourdan, S., Bernet, M., Schwartz, S., Guillot, S., Tricart, P., Chauvel, C., Dumont, T., Montagnac, G.,  
719 Bureau, S., 2012. Tracing the Oligocene-Miocene evolution of the Western Alps drainage divide with  
720 pebble petrology, geochemistry, and Raman spectroscopy of foreland basin deposits. *Journal of*  
721 *Geology* 120(6), 603–624.

- 722 Jourdan, S., Bernet, M., Tricart, P., Hardwick, E., Paquette, J. L., Guillot, S., Dumont, T., Schwartz, S.,  
723 2013. Short-lived, fast erosional exhumation of the internal western Alps during the late early  
724 Oligocene: Constraints from geothermochronology of pro-and retro-side foreland basin sediments,  
725 *Lithosphere* 5(2), 211–225.
- 726 Keller, L.M., Hess, M., Fügenschuh, B., Schmid, S.M., 2005. Structural and metamorphic evolution of the  
727 Camughera–Moncucco, Antrona and Monte Rosa units southwest of the Simplon line, Western Alps.  
728 *Eclogae Geologicae Helvetiae* 98(1), 19–49.
- 729 Kienast, J.R., Pognante, U., 1988. Chloritoid-bearing assemblages in eclogitised metagabbros of the Lanzo  
730 peridotite body (western Italian Alps). *Lithos* 21(1), 1–11.
- 731 Lafay, R., Deschamps, F., Schwartz, S., Guillot, S., Godard, M., Nicollet, C. 2013. High pressure  
732 serpentinites, a trap and release system controlled by metamorphic conditions: Example from the  
733 Piedmont zone of the western Alps. *Chemical Geology* 343, 38–54.
- 734 Lagabrielle, Y., Cannat, M., 1990. Alpine jurassic ophiolites resemble the modern central atlantic basement.  
735 *Geology* 18, 319–322.
- 736 Lanari, P., Rolland, Y., Schwartz, S., Vidal, O. Guillot, S., Tricart, P., Dumont, T., 2014. P-T-t estimation of  
737 deformation in low-grade quartz-feldspar bearing rocks using thermodynamic modeling and <sup>40</sup>Ar/<sup>39</sup>Ar  
738 dating techniques: example of the Plan-de-Phasy shear zone unit (Briançonnais Zone, Western Alps).  
739 *Terra Nova* 26, 130–138.
- 740 Lardeaux, J.M., Schwartz, S., Tricart, P., Paul, A., Guillot, S., Béthoux, N., Masson, F., 2006. A crustal-scale  
741 cross-section of the south-western Alps combining geophysical and geological imagery. *Terra Nova*  
742 18, 6, 412–422.
- 743 Lemoine, M., Bas, T., Arnaud-Vanneau, A., Arnaud, H., Dumont, T., Gidon, M., Bourbon, M., De  
744 Graciansky, P.C., Rudkiewicz, J.L., Megard-Galli, J., Tricart, P., 1986. The continental margin of the  
745 Mesozoic Tethys in the Western Alps. *Marine Petroleum Geology* 3, 179–199.
- 746 Lenze, A., Stöckhert, B., 2007. Microfabrics of UHP metamorphic granites in the Dora Maira Massif, western  
747 Alps – no evidence of deformation at great depth. *Journal of Metamorphic Geology* 25(4), 461–475.
- 748 Liou, J. G., Ernst, W. G., Zhang, R. Y., Tsujimori, T., Jahn, B. M., 2009. Ultrahigh-pressure minerals and  
749 metamorphic terranes—the view from China. *Journal of Asian Earth Sciences* 35(3), 199–231.
- 750 Little, T. A., Hacker, B. R., Gordon, S. M., Baldwin, S. L., Fitzgerald, P. G., Ellis, S., Korchinski, M., 2011.  
751 Diapiric exhumation of Earth's youngest (UHP) eclogites in the gneiss domes of the D'Entrecasteaux  
752 Islands, Papua New Guinea. *Tectonophysics* 510(1), 39–68.
- 753 Liu, Y.H., Yang, H.J., Takazawa, E., Satish-Kumar, M., You, C.F., 2015. Decoupling of the Lu-Hf, Sm-Nd,  
754 and Rb-Sr isotope systems in eclogites and a garnetite from the Sulu ultra-high pressure metamorphic  
755 terrane: Causes and implications. *Lithos* 234, 1–14.
- 756 Lombardo, B., Nervo, R., Compagnoni, R., Messiga, B., Kienast, J.R., Mével, C., Fiora, L., Piccardo, G.B.,  
757 Lanza, R., 1978, Osservazioni preliminari sulle ofiolite metamorfiche del Monviso (Alpi Occidentali).  
758 *Rendiconti della Società Italiana di Mineralogia e Petrologia* 34, 253–305.
- 759 Lyu, C., Pedersen, H., Paul, A., Zhao, L., Solarino, S. and the CIFALPS Working Group, 2017. Shear wave  
760 velocities in the upper mantle of the Western Alps: new constraints using array analysis of seismic  
761 surface waves. *Geophysical Journal International*, doi : 10.1093/gji/ggx166.
- 762 Malusà, M. G., Balestrieri, M. L., 2012. Burial and exhumation across the Alps–Apennines junction zone  
763 constrained by fission-track analysis on modern river sands. *Terra Nova* 24(3), 221–226.
- 764 Malusà, M., Mosca, P., Borghi, A., Dela Pierre, F., Polino, R., 2002. Approccio multidisciplinare per la  
765 ricostruzione dell'assetto tettono-stratigrafico e dell'evoluzione metamorfico-strutturale di un settore di  
766 catena orogenica: l'esempio dell'Alta Valle di Susa (Alpi occidentali). *Memorie della Società*  
767 *Geologica Italiana* 57(2), 249–257.

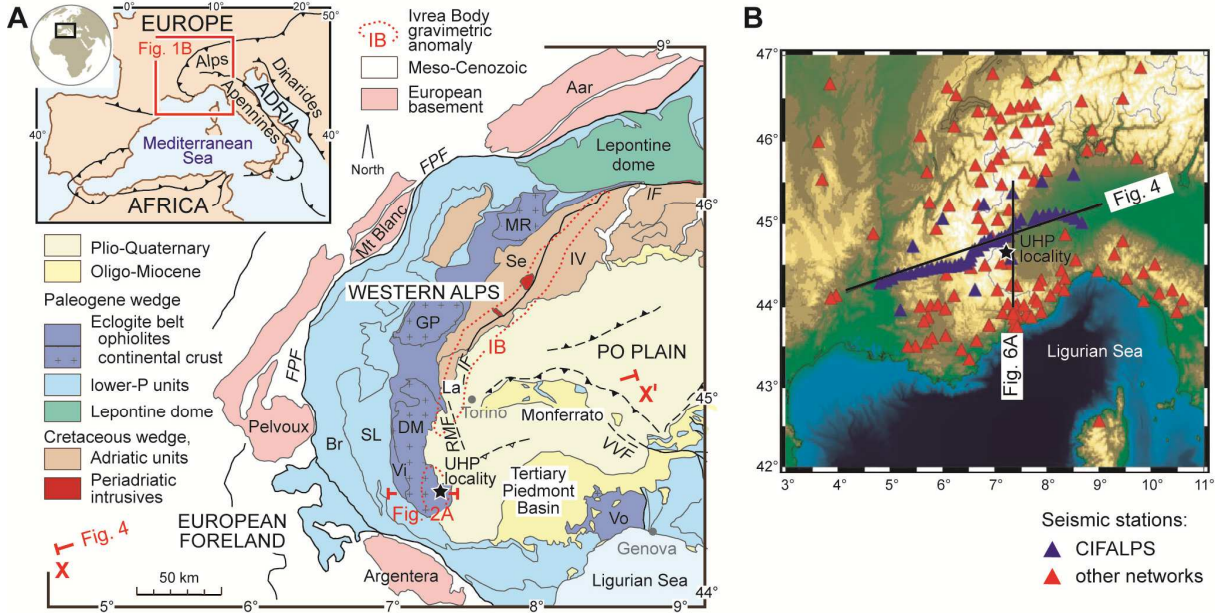
- 768 Malusà, M.G., Polino, R., Martin, S., 2005a. The Gran San Bernardo nappe in the Aosta valley (western  
769 Alps): a composite stack of distinct continental crust units. *Bulletin de la Société géologique de France*  
770 176(5), 417-431.
- 771 Malusà, M.G., Polino, R., Zattin, M., Bigazzi, G., Martin, S., Piana, F., 2005b. Miocene to Present differential  
772 exhumation in the Western Alps: Insights from fission track thermochronology. *Tectonics* 24(3).
- 773 Malusà, M.G., Polino, R., Zattin, M., 2009. Strain partitioning in the axial NW Alps since the Oligocene.  
774 *Tectonics* 28, TC3005, 1-26, doi:10.1029/2008TC002370.
- 775 Malusà, M.G., Faccenna, C., Garzanti, E., Polino, R., 2011. Divergence in subduction zones and exhumation  
776 of high-pressure rocks (Eocene Western Alps). *Earth and Planetary Science Letters* 310, 21–32.
- 777 Malusà, M.G., Faccenna, C., Baldwin, S.L., Fitzgerald, P.G., Rossetti, F., Balestrieri, M.L., Danišák, M.,  
778 Ellero, A., Ottria, G., Piromallo, C., 2015. Contrasting styles of (U)HP rock exhumation along the  
779 Cenozoic Adria-Europe plate boundary (Western Alps, Calabria, Corsica). *Geochemistry, Geophysics,*  
780 *Geosystems* 16(6), 1786–1824.
- 781 Malusà, M.G., Danišák, M., Kuhlemann, J., 2016a. Tracking the Adriatic-slab travel beneath the Tethyan  
782 margin of Corsica-Sardinia by low-temperature thermochronometry. *Gondwana Research* 31, 135-149.
- 783 Malusà, M.G., Anfinson, O.A., Dafov, L.N., Stockli, D.F., 2016b. Tracking Adria indentation beneath the  
784 Alps by detrital zircon U-Pb geochronology: Implications for the Oligocene–Miocene dynamics of the  
785 Adriatic microplate. *Geology* 44(2), 155-158.
- 786 Malusà, M.G., Zhao, L., Eva, E., Solarino, S., Paul, A., Guillot, S., Schwartz, S., Dumont, T., Aubert, C.,  
787 Salimbeni, S., Pondrelli, S., Wang Q., Zhu, R., 2017. Earthquakes in the western alpine mantle wedge.  
788 *Gondwana Research* 44, 89–95.
- 789 Marschall, H. R., Schumacher, J. C., 2012. Arc magmas sourced from mélange diapirs in subduction zones.  
790 *Nature Geoscience* 5(12), 862-867.
- 791 Mechie, J., Yuan, X., Schurr, B., Schneider, F., Sippl, C., Ratschbacher, L., Minaev, V., Gadoev, M.,  
792 Oimahmadov, I., Abdybachev, U., Moldobekov, B., Orunbaev, S., Negmatullaev, S., 2012. Crustal and  
793 uppermost mantle velocity structure along a profile across the Pamir and southern Tien Shan as derived  
794 from project TIPAGE wide-angle seismic data. *Geophysical Journal International* 188(2), 385-407.
- 795 Michard, A., Chopin, C., Henry, C., 1993. Compression versus extension in the exhumation of the Dora  
796 Maira coesite-bearing unit, Western Alps, Italy. *Tectonophysics* 221, 173–193.
- 797 Michard, A., Avigad, D., Goffé, B., Chopin, C., 2004. The high-pressure metamorphic front of the south  
798 Western Alps (Ubaye-Maira transect, France, Italy). *Schweiz. Mineral. Petrogr. Mitt.* 84, 215-235.
- 799 Müntener, O., Pettke, T., Desmurs, L., Meier, M., Schaltegger, U., 2004. Refertilisation of mantle peridotite  
800 in embryonic ocean basins: trace element and Nd isotopic evidence and implications for crust mantle  
801 relationships. *Earth and Planetary Science Letters* 221, 293–308.
- 802 Nagel, T.J., 2008. Tertiary subduction, collision and exhumation recorded in the Adula nappe, central Alps.  
803 *Geological Society, London, Special Publications* 298, 365-392.
- 804 Nicolas, A., Hirn, A., Nicolich, R., Polino, R., 1990. Lithospheric wedging in the western Alps inferred from  
805 the ECORS-CROP traverse. *Geology* 18, 587–590.
- 806 Paquette, J. L., Montel, J. M., Chopin, C., 1999. U-Th-Pb dating of the Brossasco ultrahigh-pressure  
807 metagranite, Dora-Maira massif, western Alps. *European journal of mineralogy* 11(1), 69–77.
- 808 Paul, A., Cattaneo, M., Thouvenot, F., Spallarossa, D., Béthoux, N., Fréchet, J., 2001. A three-dimensional  
809 crustal velocity model of the southwestern Alps from local earthquake tomography. *Journal of*  
810 *Geophysical Research* 106(B9), 19367-19389.
- 811 Perrone, G., Eva, E., Solarino, S., Cadoppi, P., Balestro, G., Fioraso, G., Tallone, S., 2010. Seismotectonic  
812 investigations in the inner Cottian Alps (Italian Western Alps): an integrated approach.  
813 *Tectonophysics* 496(1), 1–16.

- 814 Petersen, K.D., Buck, W.R., 2015. Eduction, extension, and exhumation of ultrahigh-pressure rocks in  
815 metamorphic core complexes due to subduction initiation. *Geochemistry, Geophysics, Geosystems*  
816 16(8), 2564-2581.
- 817 Piccardo, G.B., Müntener, O., Zanetti, A., Pettke, T., 2004. Ophiolitic peridotites of the Alpine-Apenine  
818 system: mantle processes and geodynamic relevance. *International Geology Review* 46 (12), 1119-1159.
- 819 Piccardo, G.B., Zanetti, A., Müntener, O., 2007. Melt/peridotite interaction in the Southern Lanzo peridotite:  
820 field, textural and geochemical evidence. *Lithos* 94(1), 181–209.
- 821 Plümpner, O., John, T., Podladchikov, Y.Y., Vrijmoed, J.C., Scambelluri, M., 2017. Fluid escape from  
822 subduction zones controlled by channel-forming reactive porosity. *Nature Geoscience* 10, 150-156.
- 823 Quaranta, F., Piazza, M., Vannucci, G., 2009. Climatic and tectonic control on the distribution of the Oligocene  
824 reefs of the Tertiary Piedmont Basin (NW Italy). *Italian Journal of Geosciences* 128(2), 587–591.
- 825 Quick, J. E., Sinigoi, S., Mayer, A., 1994. Emplacement dynamics of a large mafic intrusion in the lower  
826 crust, Ivrea-Verbanò Zone, northern Italy. *Journal of Geophysical Research: Solid Earth* 99(B11),  
827 21559-21573.
- 828 Reynard, B., 2013. Serpentine in active subduction zones. *Lithos* 178, 171–185.
- 829 Rubatto, D., Hermann, J., 2001. Exhumation as fast as subduction ? *Geology* 29(1), 3–6.
- 830 Rubatto, D., Hermann, J., 2003. Zircon formation during fluid circulation in eclogites (Monviso, Western  
831 Alps): implications for Zr and Hf budget in subduction zones. *Geochimica et Cosmochimica Acta*  
832 67(12), 2173–2187.
- 833 Rubatto, D., Müntener, O., Barnhoorn, A., Gregory, C., 2008. Dissolution-reprecipitation of zircon at low-  
834 temperature high-pressure conditions (Lanzo Massif, Italy). *American Mineralogist* 93, 1519–1529.
- 835 Rudnick, R. L., Fountain, D. M., 1995. Nature and composition of the continental crust: a lower crustal  
836 perspective. *Reviews of Geophysics* 33, 267-309.
- 837 Scafidi, D., Solarino, S., Eva, C., 2006. Structure and properties of the Ivrea body and of the Alps-Apennines  
838 systems as revealed by local earthquake tomography. *Bollettino Geofisica Teorica Applicata* 47, 497–514.
- 839 Scafidi, D., Solarino, S., Eva C., 2009. P wave seismic velocity and Vp/Vs ratio beneath the Italian Peninsula  
840 from local earthquake tomography. *Tectonophysics* 465, 1–23.
- 841 Scambelluri, M., Tonarini, S., 2012. Boron isotope evidence for shallow fluid transfer across subduction  
842 zones by serpentinized mantle. *Geology* 40, 907–910.
- 843 Scambelluri, M., Müntener, O., Hermann, J., Piccardo, G.B., Trommsdorff, V., 1995. Subduction of water  
844 into the mantle: history of an Alpine peridotite. *Geology* 23, 459–462
- 845 Scambelluri, M., van Roermund, H. L., Pettke, T., 2010. Mantle wedge peridotites: fossil reservoirs of deep  
846 subduction zone processes: inferences from high and ultrahigh-pressure rocks from Bardane (Western  
847 Norway) and Ulten (Italian Alps). *Lithos* 120(1), 186-201.
- 848 Schaltegger, U., Brack, P., 2007. Crustal-scale magmatic systems during intracontinental strike-slip  
849 tectonics: U, Pb and Hf isotopic constraints from Permian magmatic rocks of the Southern Alps.  
850 *International Journal of Earth Sciences* 96(6), 1131–1151.
- 851 Schmid, S.M., Kissling, E., 2000. The arc of the western Alps in the light of geophysical data on deep crustal  
852 structure. *Tectonics* 19, 62–85.
- 853 Schmid, S. M., Fügenschuh, B., Kissling, E., Schuster, R., 2004. Tectonic map and overall architecture of the  
854 Alpine orogen. *Eclogae Geologicae Helvetiae* 97, 93-117.
- 855 Schmid, S.M., Kissling, E., Diehl, T., van Hinsbergen, D., Molli, G., 2017. Ivrea mantle wedge, arc of the  
856 Western Alps, and kinematic evolution of the Alps–Apennines orogenic system. *Swiss Journal of*  
857 *Geosciences* 110, 581-612.
- 858 Schwartz, S., Lardeaux, J.M., Guillot, S., Tricart, P., 2000. Diversité du métamorphisme éclogitique dans le  
859 massif ophiolitique du Monviso (Alpes occidentales, Italie). *Geodinamica Acta* 13, 169-188.

- 860 Schwartz, S., Allemand, P., Guillot, S. 2001. Numerical model of the effect of serpentinites on the  
861 exhumation of eclogitic rocks: insights from the Monviso ophiolitic massif (Western Alps).  
862 *Tectonophysics* 342, 193–206.
- 863 Schwartz, S., Tricart, P., Lardeaux, J.M., Guillot, S., Vidal, O. 2009. Late tectonic and metamorphic  
864 evolution of the Piedmont accretionary wedge (Queyras Schistes lustrés, western Alps): Evidences for  
865 tilting during Alpine collision. *Geological Society of America Bulletin* 121, 502–518.
- 866 Schwartz, S., Gautheron, C., Audin, L., Dumont, T., Nomade, J., Barbarand, J., 2017. Foreland exhumation  
867 controlled by crustal thickening in the Western Alps. *Geology* 45(2), 139–142.
- 868 Solarino, S., Kissling, E., Sellami, S., Smriglio, G., Thouvenot, F., Granet, M., Bonjer, K.P., Slejko, D.,  
869 1997. Compilation of a recent seismicity data base of the greater Alpine region from several  
870 seismological networks and preliminary 3D tomographic results. *Annals of Geophysics* 40(1).
- 871 Sue, C., Delacou, B., Champagnac, J.D., Allanic, C., Tricart, P., Burkhard, M., 2007. Extensional  
872 neotectonics around the bend of the Western/Central Alps: an overview. *International Journal of Earth  
873 Sciences* 96(6), 1101–1129.
- 874 Thurber, C.H., 1983. Earthquake locations and three-dimensional crustal structure in the Coyote Lake area,  
875 central California. *Journal of Geophysical Research: Solid Earth* 88(B10), 8226–8236.
- 876 Tricart, P., Schwartz, S., 2006. A north - south section across the Queyras Schistes lustrés (Piedmont zone,  
877 Western Alps) : syncollision refolding of a subduction wedge. *Eclogae Geologicae Helveticae* 9, 429–442.
- 878 Tricart, P., Schwartz, S., Sue, C., Lardeaux, J.M., 2004. Differential exhumation in the inner western Alpine  
879 arc evidenced by late normal faulting (eastern Queyras Schistes lustrés). *Journal of Structural Geology*  
880 26, 1633–1645.
- 881 Tricart, P., van der Beek, P., Schwartz, S., Labrin, E., 2007. Diachronous late-stage exhumation across the  
882 western Alpine arc: constraints from apatite fission-track thermochronology between the Pelvoux and  
883 Dora-Maira Massifs. *Journal of the Geological Society* 164(1), 163–174.
- 884 Vernon, A.J., van der Beek, P.A., Sinclair, H.D., Rahn, M.K., 2008. Increase in late Neogene denudation of  
885 the European Alps confirmed by analysis of a fission-track thermochronology database. *Earth and  
886 Planetary Science Letters* 270, 316–329.
- 887 Vignaroli, G., Faccenna, C., Jolivet, L., Piromallo, C., Rossetti, F. (2008). Subduction polarity reversal at the  
888 junction between the Western Alps and the Northern Apennines, Italy. *Tectonophysics* 450(1), 34–50.
- 889 Virieux, J., 1991. Fast and accurate ray tracing by Hamiltonian perturbation. *Journal of Geophysical  
890 Research: Solid Earth* 96(B1), 579–594.
- 891 van Roermund, H. (2009). Mantle-wedge garnet peridotites from the northernmost ultra-high pressure domain  
892 of the Western Gneiss Region, SW Norway. *European Journal of Mineralogy* 21(6), 1085–1096.
- 893 Wagner, M., Kissling, E., Husen, S., 2012. Combining controlled-source seismology and local earthquake  
894 tomography to derive a 3-D crustal model of the western Alpine region. *Geophysical Journal  
895 International* 191(2), 789–802.
- 896 Wang, Q., Ji, S., Salisbury, M. H., Xia, B., Pan, M., Xu, Z., 2005. Pressure dependence and anisotropy of P-  
897 wave velocities in ultrahigh-pressure metamorphic rocks from the Dabie–Sulu orogenic belt (China):  
898 implications for seismic properties of subducted slabs and origin of mantle reflections. *Tectonophysics*  
899 398(1), 67–99.
- 900 Warren, C.J., 2013. Exhumation of (ultra-) high-pressure terranes: Concepts and mechanisms. *Solid Earth*  
901 4(1), 75–92.
- 902 Weiss, T., Siegesmund, S., Rabbel, W., Bohlen, T., Pohl, M., 1999. Seismic velocities and anisotropy of the  
903 lower continental crust. A Review. *Pure Applied Geophysics* 156, 97–122.
- 904 Yamato, P., Burov, E., Agard, P., Le Pourhiet, L., Jolivet, L., 2008. HP-UHP exhumation during slow  
905 continental subduction: Self-consistent thermodynamically and thermomechanically coupled model  
906 with application to the Western Alps. *Earth and Planetary Science Letters* 271(1), 63–74.

- 907 Zanchetta, S., Malusà, M.G., Zanchi, A., 2015. Precollisional development and Cenozoic evolution of the  
908 Southalpine retrobelt (European Alps). *Lithosphere* 7, 662-681.
- 909 Zeitler, P.K., Koons, P.O., Bishop, M.P., Chamberlain, C.P., Craw, D., et al., 2001. Crustal reworking at  
910 Nanga Parbat, Pakistan: metamorphic consequences of thermal–mechanical coupling facilitated by  
911 erosion, *Tectonics*, 20, 712–728.
- 912 Zhao, L., Paul, A., Guillot, S., Solarino, S., Malusà, M.G., Zheng, T., Aubert, C., Salimbeni, S., Dumont, T.,  
913 Schwartz, S., Zhu, R., Wang, Q., 2015. First seismic evidence for continental subduction beneath the  
914 Western Alps. *Geology* 43, 815-818.
- 915 Zhao, L., Paul, A., Malusà, M.G., Xu, X., Zheng, T., Solarino, S., Guillot, S., Schwartz, S., Dumont, T.,  
916 Salimbeni, S., Aubert, C., Pondrelli, S., Wang, Q., Zhu, R., 2016a. Continuity of the Alpine slab  
917 unraveled by high-resolution P wave tomography. *Journal of Geophysical Research: Solid Earth* 121,  
918 8720–8737.
- 919 Zhao, L., Paul, A., Solarino S., 2016b. Seismic network YP: CIFALPS temporary experiment (China-Italy-  
920 France Alps seismic transect). RESIF - Réseau Sismologique et géodésique Français. Seismic  
921 Network. doi:10.15778/RESIF.YP2012.
- 922 Zhao, L., Xu, X., Malusà, M.G., 2017. Seismic probing of continental subduction zones. *Journal of Asian*  
923 *Earth Sciences* 145, 37-45.  
924

Figure 1



926  
927

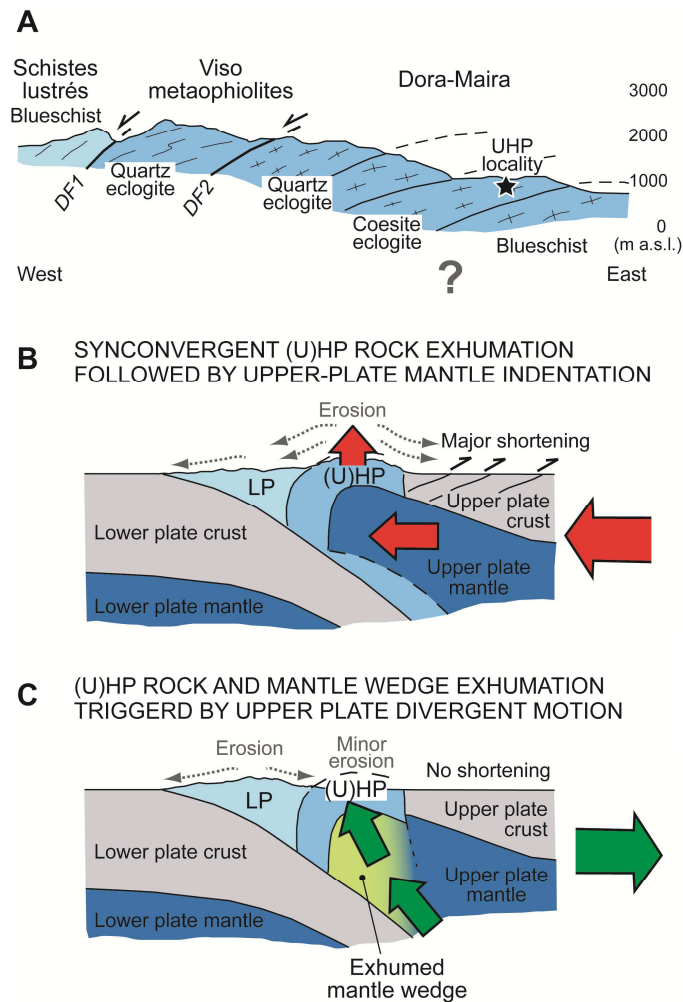
**Figure 1:** A) Tectonic sketch map showing the (U)HP domes of the Western Alps (dark blue), the gravimetric anomaly of the Ivrea body (0 mGal isoline in red), and the location of the CIFALPS transect (X-X'). Acronyms: Br, Briançonnais; DM, Dora-Maira; FPF, Frontal Pennine Fault; GP, Gran Paradiso; IF, Insubric Fault; IV, Ivrea-Verbano; La, Lanzo; MR, Monte Rosa; RMF, Rivoli-Marene deep fault; Se, Sesia-Lanzo; SL, Schistes lustrés; Vi, Viso; Vo, Voltri; VVF, Villalvernia-Varzi Fault. The black star marks the Brossasco-Isasca UHP locality. B) Seismic stations utilized in this work (blue = CIFALPS; red = other networks) and location of tomographic cross sections (black lines).

936



937  
938

Figure 2

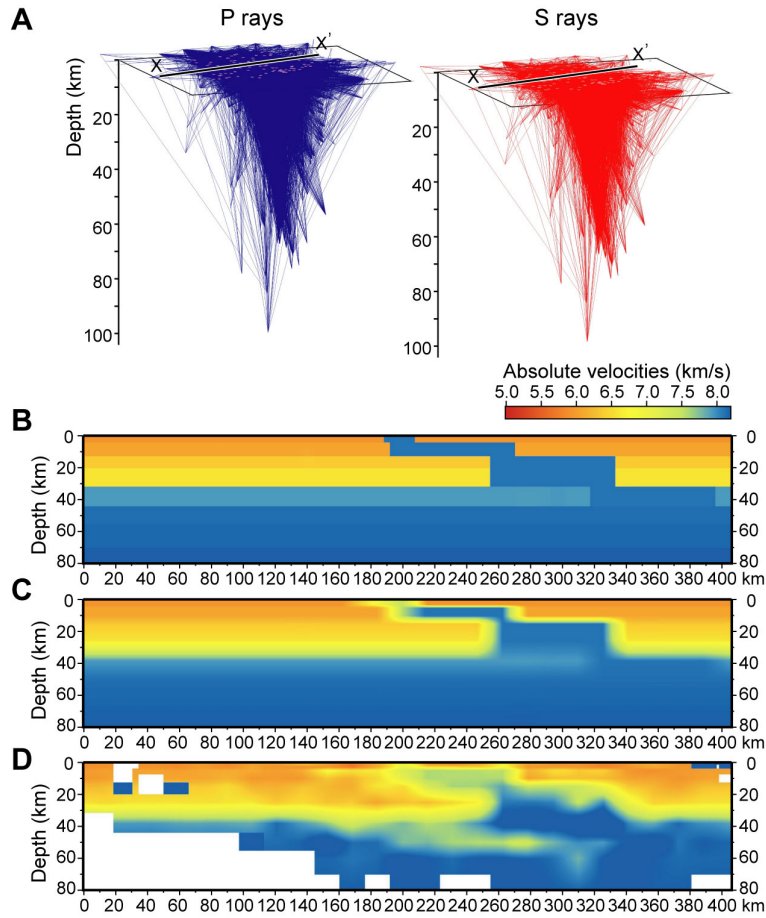


939  
940  
941  
942  
943  
944  
945  
946  
947  
948  
949  
950  
951  
952  
953  
954  
955  
956  
957

**Figure 2: A)** Geologic cross-section of the Dora-Maira (U)HP dome (see location in Fig. 1A; based on Avigad et al., 2003; Lardeaux et al., 2006). **B, C)** Alternative scenarios of mantle involvement in (U)HP orogenic belts. In (B), synconvergent exhumation of (U)HP rocks (e.g., Butler et al., 2013), possibly associated with deep duplex formation (Schmid et al., 2017), is followed by indentation of the upper-plate mantle beneath the accretionary wedge, with consequent fast erosion of the (U)HP dome and major tectonic shortening in the upper plate (e.g., Béthoux et al., 2007). Seismic velocities in the upper-plate mantle are similar beneath the orogenic belt and in the hinterland, as indicated by the uniform dark blue colour. In (C), divergence between upper plate and accretionary wedge triggers the exhumation of (U)HP rocks (Malusà et al., 2011) and the emplacement of serpentinitized mantle-wedge rocks at shallow depth. Erosion on top of the (U)HP dome is minor at this stage, and shortening is negligible. Because of widespread serpentinitization of the mantle wedge during subduction, seismic velocities will be lower in the mantle-wedge rocks beneath the (U)HP dome (as indicated by the pale green colour), and higher in the adjoining dry mantle rocks of the upper plate (dark blue).

958  
959

Figure 3

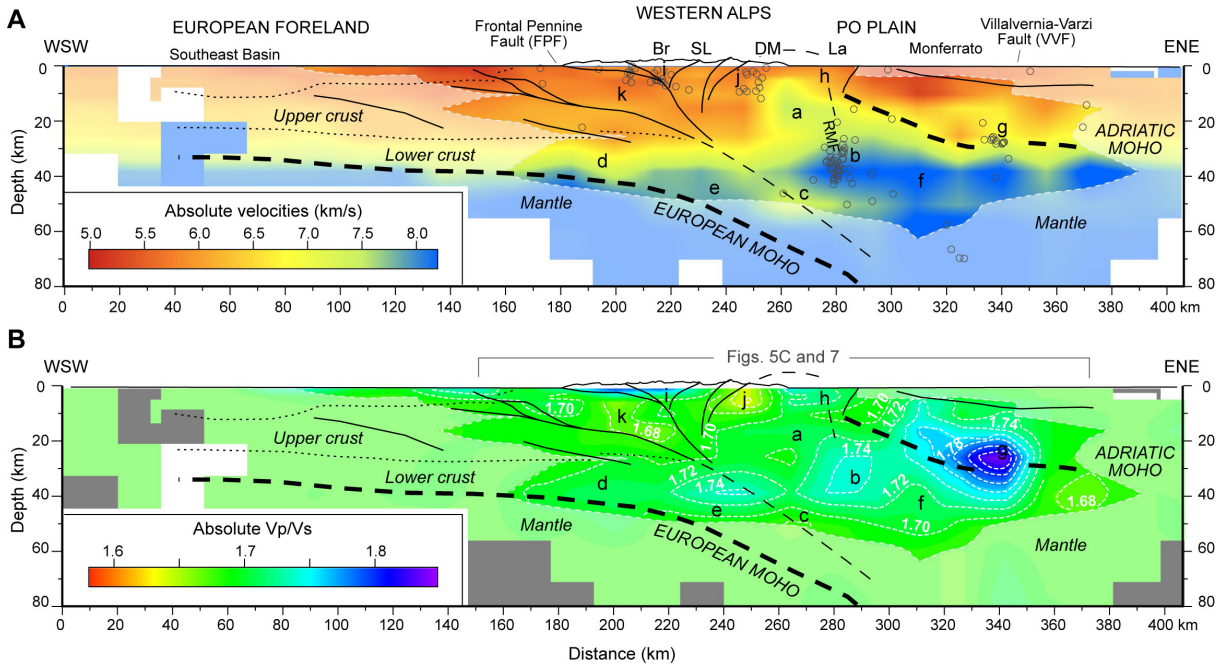


960  
961  
962  
963  
964  
965  
966  
967  
968  
969  
970  
971  
972

**Figure 3.** A) Three-dimensional P and S ray coverage based on the seismic events considered in this study (X-X' indicates the CIFALPS transect, see Fig. 1). B) Imposed stairwell geometry along the CIFALPS transect for testing the resolution capability of the coupling between seismic dataset and inversion setup. C) Same geometry after interpolation by the algorithm used in SIMULPS, which introduces a smoothing and a thin band of fake colors around the anomalies. D) Reconstruction test showing that the shape of the imposed stairwell structure is well reproduced using our dataset, but the high velocities in the uppermost 10 km are converted to lower values (as less as 0.5 km/s); the weak vertical and horizontal periodic stripes of yellow color at 50 km depth within the blue area are artifacts; white areas are not sampled.

973  
974

Figure 4

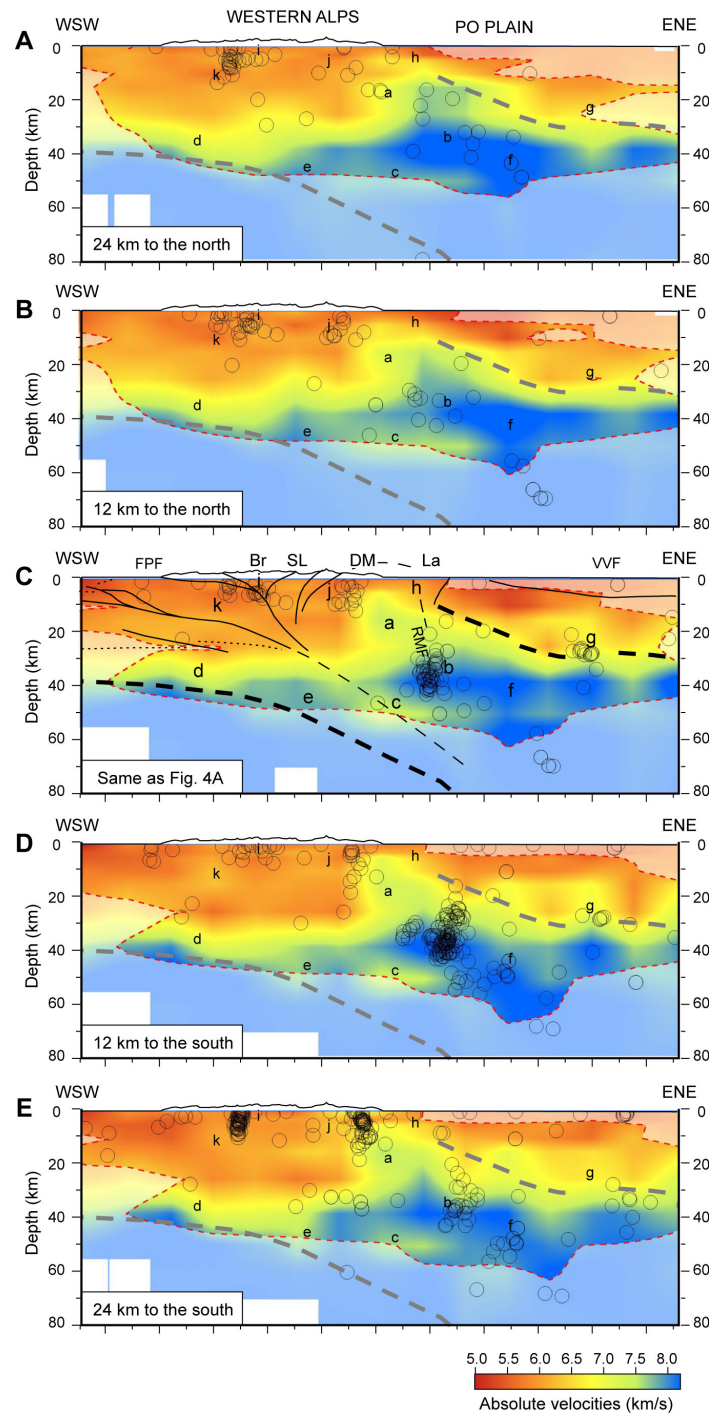


975  
976  
977  
978  
979  
980  
981  
982  
983  
984  
985  
986  
987

**Figure 4:** Tomographic cross sections along the CIFALPS transect. A) Absolute Vp velocity. The velocity structure beneath the Dora-Maira (U)HP dome is well resolved down to 50-60 km depth (acronyms as in Fig. 1A); areas with resolution diagonal elements  $<0.1$  are masked, white areas are not sampled; letters a to k indicate regions of the model discussed in the main text; black circles indicate earthquakes as located with the 3D model; black lines and text in italics indicate the main tectonic features previously inferred from receiver function analysis (Zhao et al., 2015; Malusà et al., 2017, see Fig. 7B). Note the prominent high velocity body (labelled with “a”) located right below the Dora-Maira (U)HP dome. The vertical and horizontal periodic stripes of yellow color at 50 km depth are artifacts, as attested by the reconstruction test of Fig. 3D. B) Vp/Vs ratios. White dashed lines are isolines of equal Vp/Vs, grey areas are not sampled (other keys as in frame A).

988  
989

Figure 5

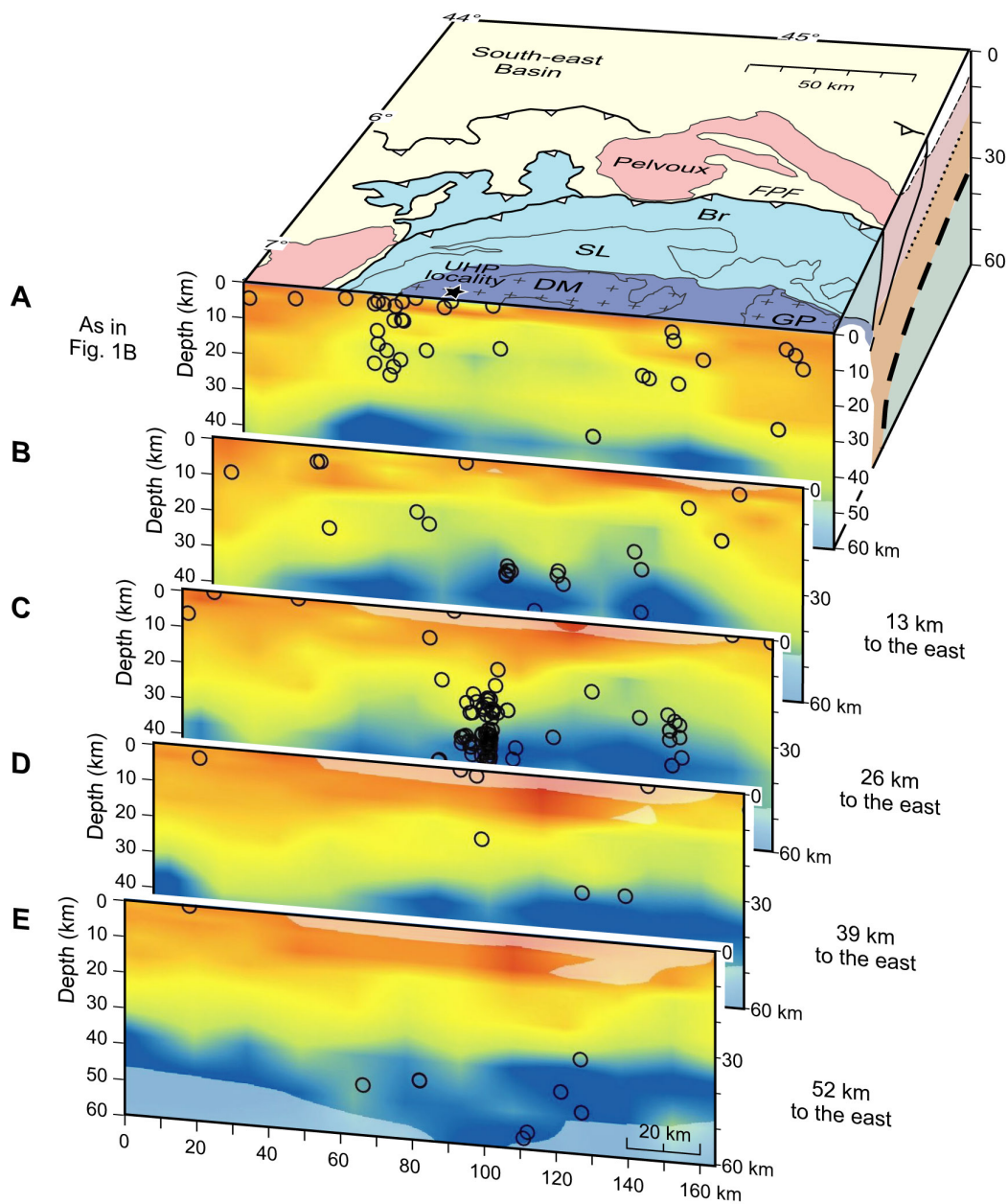


990  
991  
992  
993  
994  
995  
996  
997  
998

**Figure 5:** Lateral variations in Vp velocity in the mantle wedge as shown in a series of WSW-ENE cross-sections lying to the north (A, B) and to the south (D, E) of the main CIFALPS transect (C). The high velocity body labelled with “a” progressively disappears moving to the north. Black circles are projected hypocentres located within  $\pm 5$  km distance off the profiles. The thick dashed lines, reported in all sections for comparison, indicate the European and Adriatic Mohos inferred from receiver function analysis (cf. Fig. 7B). Other keys as in Fig. 4.

999  
1000  
1001

Figure 6

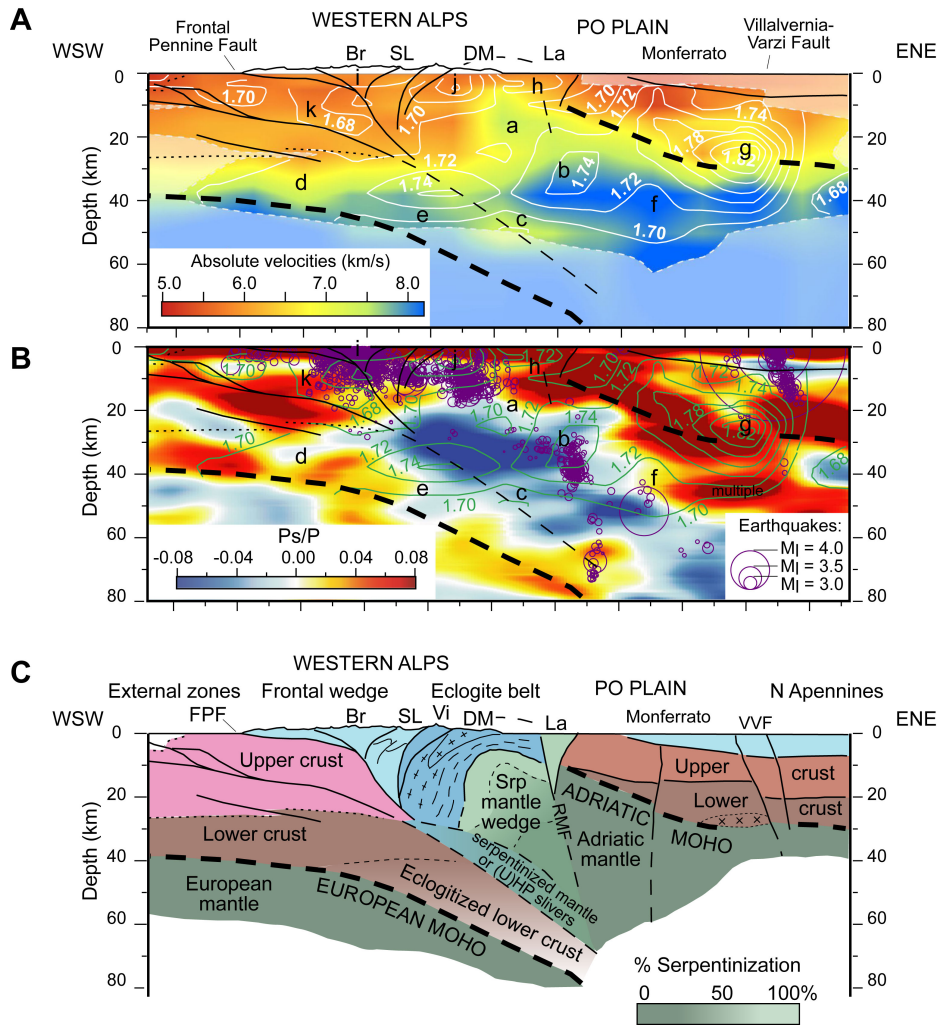


1002  
1003  
1004  
1005  
1006  
1007  
1008  
1009

**Figure 6:** Lateral variations in  $V_p$  velocity beneath the Dora-Maira (U)HP dome, as shown in a series of N-S cross-sections from the mountain range to the Po Plain. Black circles are projected hypocentres located within  $\pm 3$  km distance off the profiles. The high-velocity body labelled with “a” in Figs. 4 and 5 is exclusively found beneath the Dora-Maira dome (see cross section A) and progressively disappears towards the east. Acronyms as in Fig. 1.

1010  
1011

Figure 7

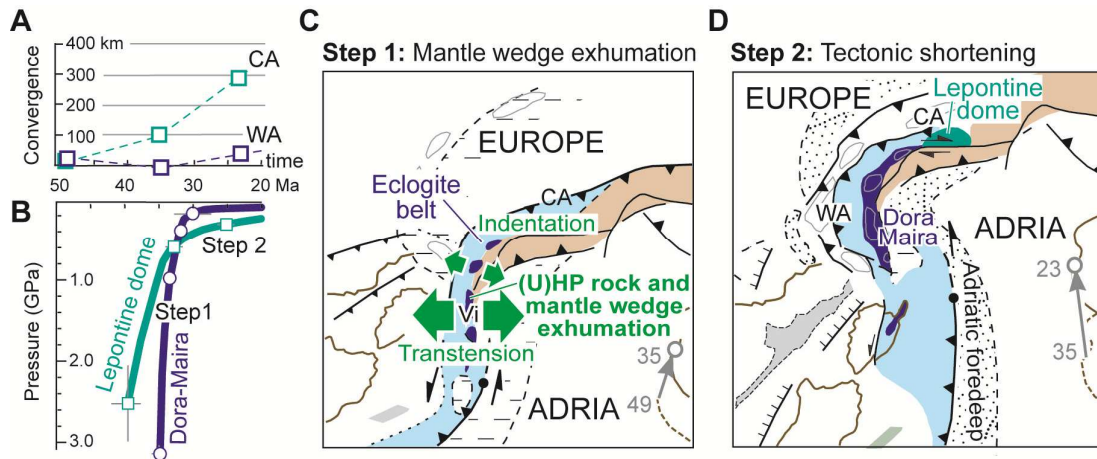


1012  
1013  
1014  
1015  
1016  
1017  
1018  
1019  
1020  
1021  
1022  
1023

**Figure 7:** Synthesis of geophysical data (A, B) and inferred mantle wedge structure (C). Black lines in A and B are tectonic features based on receiver function analysis (colors in B indicate positive- and negative-polarity Ps-converted phases, Zhao et al., 2015); contours are isolines of equal  $V_p/V_s$ ; purple circles in B are earthquakes recorded since 1990 (Malusà et al., 2017). The amount of serpentinitization in C, in the mantle wedge underlying the Dora-Maira (U)HP dome, is inferred from seismic velocities (Reynard, 2013). Note the consistency between structures unravelled by local (A) and teleseismic (B) events. Acronyms as in Fig. 1, letters a to k as in Fig. 4.

1024  
1025  
1026

Figure 8



1027  
1028  
1029  
1030  
1031  
1032  
1033  
1034  
1035

**Figure 8:** Geodynamic framework of mantle wedge exhumation. **A)** Trench-normal component of Adria-Europe relative motion in the Central (CA) and Western Alps (WA) segments of the Alpine subduction zone (Malusà et al., 2015). **B)** Pressure-time exhumation paths (Dora-Maira: Chopin et al., 1991; Rubatto and Hermann, 2001; Lepontine dome: Becker, 1993; Gebauer, 1996; Brouwer et al., 2004; Nagel, 2008). **C,D)** Late Eocene transtension leading to (U)HP rock and mantle wedge exhumation, and subsequent tectonic shortening in the early Oligocene; grey arrows indicate Adria motion relative to Europe (modified after Malusà et al., 2015).